AD-A099 311 HUGHES RESEARCH LABS MALIBU CA F/G 17/8
MECHANICAL STRESS IN THIN FILMS.(U)
MAR 81 W PEDINOFF, D MAYER, R HENDERSON F30602-79-C-0163
UNCLASSIFIED RADC-TR-81-22 NL

1 OF 1
AD A
099311

END
DATE FILMED
6-81
DTIC

RADC-TR-81-22
Final Technical Report
March 1981

MECHANICAL STRESS IN THIN FILMS

Hughes Research Laboratories

M. Pedinoff
D. Mayer
R. Henderson

ROME AIR DEVELOPMENT CENTER
Air Force Systems Command
Griffiss Air Force Base, New York 13441

This report has been reviewed by the RADC Public Affairs Office (PA) and is releasable to the National Technical Information Service (NTIS). At NTIS it will be releasable to the general public, including foreign nations.

RADC-TR-81-22 has been reviewed and is approved for publication.

APPROVED: Clyde H. Lane

CLYDE H. LANE
Project Engineer

APPROVED: David C. Luke

DAVID C. LUKE, Colonel, USAF
Chief, Reliability & Compatibility Division

FOR THE COMMANDER: John P. Huss

JOHN P. HUSS
Acting Chief, Plans Office

If your address has changed or if you wish to be removed from the RADC mailing list, or if the addressee is no longer employed by your organization, please notify RADC (RBRP) Griffiss AFB NY 13441. This will assist us in maintaining a current mailing list.

Do not return this copy. Retain or destroy.

UNCLASSIFIED

SECURITY CLASSIFICATION OF THIS PAGE (When Data Entered)

REPORT DOCUMENTATION PAGE

READ INSTRUCTIONS BEFORE COMPLETING FORM

1. REPORT NUMBER: RADC-TR-81-22	2. GOVT ACCESSION NO.: AD-A099311
3. RECIPIENT'S CATALOG NUMBER	
4. TITLE (and Subtitle): MECHANICAL STRESS IN THIN FILMS	5. TYPE OF REPORT & PERIOD COVERED: Final Technical Report,
6. PERFORMING ORG. REPORT NUMBER: N/A	
7. AUTHOR(s): M. Pedinoff, D. Mayer, R. Henderson	8. CONTRACT OR GRANT NUMBER(s): F30602-79-C-0163
9. PERFORMING ORGANIZATION NAME AND ADDRESS: Hughes Research Laboratories, 3011 Malibu Canyon Road, Malibu CA 90265	10. PROGRAM ELEMENT, PROJECT, TASK AREA & WORK UNIT NUMBERS: 61102F, 2306J402
11. CONTROLLING OFFICE NAME AND ADDRESS: Rome Air Development Center (RBRP), Griffiss AFB NY 13441	12. REPORT DATE: March 1981
	13. NUMBER OF PAGES: 93
14. MONITORING AGENCY NAME & ADDRESS (if different from Controlling Office): Same	15. SECURITY CLASS. (of this report): UNCLASSIFIED
	15a. DECLASSIFICATION/DOWNGRADING SCHEDULE: N/A

16. DISTRIBUTION STATEMENT (of this Report)

Approved for public release; distribution unlimited.

17. DISTRIBUTION STATEMENT (of the abstract entered in Block 20, if different from Report)

Same

18. SUPPLEMENTARY NOTES

RADC Project Engineer: Clyde H. Lane (RBRP)

19. KEY WORDS (Continue on reverse side if necessary and identify by block number)

Silicon dioxide	Ellipsometry
Thin films	Silicon-on-sapphire
Microelectronics	Stress measurement

20. ABSTRACT (Continue on reverse side if necessary and identify by block number)

A multi-angle ellipsometry technique has been developed. The elements are: Measure Δ and ψ for several angles of incidence. Then compare the data with theoretical values which have been calculated from a model that predicts the optical properties for a system comprising several thin film layers on an reflecting substrate. Each film layer has some anisotropy (stress) and optical constants: iterate the model →

DD FORM 1 JAN 73 1473 EDITION OF 1 NOV 65 IS OBSOLETE

UNCLASSIFIED

SECURITY CLASSIFICATION OF THIS PAGE (When Data Entered)

parameters to obtain the best fit with the measured and theoretical values for Δ and Ψ.

This technique has been applied with success to SiO_2 and silicon-on-sapphire thin films. The data reveal a 6 Å thick inner layer between the SiO_2 film and the silicon substrate. The films have various stress values in the 10^9 dyne/cm^2 range. Strong stress (up to 10^{10} dyne/cm^2) is found in silicon-on-sapphire. Three SOS samples were graded for optical quality – the degree of perfection was inversely related to the amount of stress found.

EVALUATION

Hughes has done an excellent job in applying the ellipsometer to the problem of nondestructive measurement of stress in silicon dioxide on silicon and silicon on sapphire. The development of multiangle ellipsometry for this purpose and to measure the interphase layer between the film and its substrate was an exclusive Hughes development. They not only investigated and stressed the strong points of the technique, however, they also investigated the limitation of the method. As a result of this contract a significant step forward has been made in ellipsometry and its application to nondestructive in-line testing. The technique permits self-standardization in that no external standards are required for comparison. It can be applied to the study of corrosion, impurity segregation, multilayer films, etc. as well as oxidation and heteroepitaxy. The possiblity of obtaining information on defect densities in heteroepitaxy films has been demonstrated as well.

The Air Force as well as the other services can make use of this tool in a myriad of ways. In particular the method may be applied to wafer selection for silicon on sapphire processing. We expect the result will be an improvement in yield, reliability and cost of SOS devices. This, of course, is the ultimate goal of our basic research program in support of the RADC technical program objective for solid state device reliability.

Clyde H. Lane

CLYDE H. LANE
Project Engineer

TABLE OF CONTENTS

SECTION PAGE

LIST OF ILLUSTRATIONS

SECTION 1

INTRODUCTION AND OVERVIEW

A. BACKGROUND

The increasing stringency of the speed, power, and density requirements of military systems over the past decade has contributed to a rapid reduction in the typical feature size of IC components and to the development of high-performance technologies such as CMOS/SOS and I^2L. To allow semiconductor technologies to evolve toward even smaller feature sizes and improved performance characteristics, a better understanding of the physical principles controlling semiconductor device behavior is crucial. Particular emphasis must be placed on understanding second-order phenomena: their influence, which could be neglected for relatively large device dimensions, increases rapidly as IC feature sizes are scaled to submicrometer dimensions.

Mechanical stress in silicon and silicon dioxide thin films is an example of such a phenomenon. Large stresses exist in thermally oxidized silicon[1,2] and at the interface between silicon and sapphire in SOS systems.[3,4] A correlation between Si/SiO_2 interface state density and both stress and stress history has been suggested.[5] Defect density in oxide windows may be a stress-dependent phenomenon. It is also known that stress in SOS films can significantly affect carrier mobility,[6] energy band gap shift,[7] and defect density at the material interface. But in spite of such evidence, silicon IC design and fabrication techniques have evolved with little or no regard for their effects on film stress and subsequent circuit performance.

This report contains the results of a 12-month program, entitled Mechanical Stress Effects in Silicon Devices, to study the correlation between stress in silicon/silicon dioxide and silicon-on-sapphire systems and the electrical properties of silicon and SOS devices, including those factors during epitaxial growth and thermal oxidation of silicon films that influence stress. We believe that this study was a crucial companion effort to the VHSIC program under way in the Department of Defense. Investigation into the role of interface stress in influencing such IC cost- and performance-related parameters as defect density, interface state density, and carrier mobility is

essential to the complete understanding of device and circuit operation at the submicrometer dimensions required for VHSIC.

B. TECHNICAL DISCUSSION

1. Stress In Thermally Grown Silicon Oxide

a. Growth Conditions

Silicon oxide films on silicon are known to become compressed when thermally grown and cooled as a result of the difference in thermal expansion coefficients between the two films.[1,2] The magnitude of the resultant stress in the oxide has been measured[1] in the range 1 to 5 x 10^9 dyn/cm^2. In general, samples oxidized in wet O_2 exhibited less stress than those oxidized in dry O_2.[1] A residual hydroxyl concentration in the oxide, which may increase its thermal expansion coefficient, was suggested to explain this phenomenon. Oxide stress was observed to increase with quench rate. Viscous flow of the oxide may cause thermal equilibrium to be reached at a temperature below the growth temperature when the samples are slow-cooled. The oxide stress would then be proportional to the difference between room temperature and the equilibrium temperature, rather than between room temperature and the higher growth temperature, thereby explaining the stress reduction. It has also been shown[5] that residual stress is lower in oxides grown at lower temperatures as a result of the reduced cooling range.

b. Stress Relaxation

Because thermally grown silicon oxides exhibit viscous flow at temperatures as low as 965°C, it appears possible that an anneal of an oxide grown at a higher temperature might reduce residual stress by allowing thermal equilibrium to be reached between the oxide and the silicon substrate at the lower temperature. It has been suggested,[8] however, that a significant number of interface states may be created when stress relaxation is caused by viscous flow.

Stress relief in deposited silicon oxide films has also been observed[9] after ultraviolet irradiation. The stress relaxation mechanism here is believed[9] to be the mobilization and redistribution of gettered oxygen atoms in the oxide film resulting from the absorption of radiation.

c. Interface States

A relation between stress and interface states in the Si/SiO_2 system has not been clearly established. Whelan et al.[1] found no correlation between interface state density and either residual stress or induced stress up to sample fracturing. Lane,[5] on the other hand, has found evidence that the interface state density decreases as stress increases. He attributes interface states to vacancies at the Si/SiO_2 interface and correlates the reduction in interface state density to the disappearance of vacancies during compressive stress.

It has also been demonstrated[5,8] that the reduction of the interface stress through annealing can give rise to an increase in surface state density. Lane[5] attributes this to the reappearance of vacancies at the interface as the compression is reduced, while Ernisse and Derbenwick[8] postulate the creation of hole traps near the Si/SiO_2 interface that arise during the viscous flow of the annealing oxide. The hole trap model also explains the flatband voltage shift observed in stress-relieved oxides under ionizing radiation. In this model, a net positive charge accumulates in the hole traps at the interface whenever an electron-hole pair is created by an impinging high-energy photon. This interface charge then causes the observed flatband shift.

d. Defect Density

Another crucial topic in silicon IC fabrication is the relation between stress at the Si/SiO_2 or the Si/Al_2O_3 interfaces and the density of silicon surface defects. This can affect circuit performance and reliability through reduced surface breakdown voltage, decreased carrier mobility, surface conduction mechanisms, and surface-to-substrate shorts. The importance of this problem is expected to increase significantly as the smaller feature sizes and greater packing densities required for VLSI and VHSI increase the stringency of material defect requirements.

A study of the effects of stress on defect density in windows opened in thermally grown SiO_2 can serve as a basis for the evaluation of stress-induced defects. A further advantage of such an investigation is the ability to consider defect density as a function of window size. Since the etching

of windows in thermal oxides changes the stress distribution in the exposed areas,[10] there should be a correlation between window size and defect density. The distribution of defects is also expected to vary across the window due to the discontinuity in interfacial stress at the window edges. This may be of particular interest in VHSI and VLSI circuits where the reduced size of the contact windows will significantly increase the window perimeter-to-area ratio, thereby leveraging the importance of window edge-related defects.

Stress-induced defects at the Si/SiO_2 interface can increase surface leakage in p-n junction devices by acting as minority carrier recombination sites. Surface carrier mobility is also reduced due to scattering from defect sites. Surface defects can also cause premature junction breakdown by distorting the electric field distribution in the junction, thereby enhancing avalanche multiplication. Each of these effects represents a potential circuit failure mechanism the importance of which must be evaluated and minimized before any VHSI or VLSI technology can be developed.

2. Stress In Silicon-On-Sapphire

a. Growth Conditions

Stress in epitaxial silicon-on-sapphire has been measured[3] to be as high as 1×10^{10} dyn/cm^2. The source of this interfacial stress lies both in the difference in thermal expansion coefficients between the two materials as the wafers are cooled from the growth temperature, as well as in an inherent mismatch between the lattices of (100) silicon and $[1\bar{1}02]$ sapphire.

Although the lattice mismatch at the SOS interface adds a degree of complexity that was lacking in the Si/SiO_2 system, it appears possible that considerable stress reduction can be achieved at the SOS interface through careful control of the epitaxial growth process. Moreover, the lack of a technique for rapidly evaluating film quality in SOS materials has been an industry-wide problem. The quality of SOS films has been measured with Rutherford backscattering (RBS) and double-reflection X-ray diffraction. But, these techniques are tedious and time consuming. The ellipsometric stress measurement technique described in Section 2 can offer a rapid and accurate evaluation of the starting material for SOS devices.

b. Mobility

The piezoresistance effect, in which carrier mobility in the Si lattice is changed when stresses are applied, has been recognized in bulk Si for many years. Hughes and Thorsen[6] have demonstrated that the same principle applies in the SOS system by showing a good correlation between the anisotropies in residual stress and Hall mobility in SOS thin films.

A direct correlation between stress and mobility through a piezoresistance effect is complicated in SOS structures by the interrelationship between stress and defect formation at the SOS interface. It is known that defect scattering can significantly reduce carrier mobility near the Si/Al_2O_3 interface.

c. Energy Band Gap

Changes in the energy band gap of semiconductors as pressure is applied have been studied by various authors. Bulthuis[7] demonstrated this correlation in Si by observing changes in reverse current in p-n junction diodes as a function of applied pressure. Bulthuis assumed a linear relationship between band gap shift and pressure and was able to measure a proportionality constant of approximately -5×10^{-6} eV $kg^{-1}cm^2$. If it is assumed that this proportionality constant applies for the case of silicon-on-sapphire and that stresses on the order of 10^{10} dyn/cm^2 are observed, then a band gap shift of approximately -0.05 eV is expected.

d. Defect Density

The large stresses observed in SOS thin films are expected to affect defect nucleation and propagation at the Si/Al_2O_3 interface. Although electrical interaction between current carriers and SOS interface defects is generally avoided by restricting current flow near the surface in SOS devices, some interaction must occur. In particular, current conduction on Si island edges requires interaction with these interface defects. The problems associated with a very high defect concentration at the Si/Al_2O_3 interface have been avoided in previous CMOS/SOS circuits by building these circuits on relatively thick films (>0.5 μm), where good material surface properties can be maintained, and by maximizing the ratio of surface-to-edge conduction in order to minimize defect-related edge effects. However, the

reduction in feature size and the increase in packing density associated with the VHSI and VLSI design trends in today's semiconductor industry will require both a thinning of SOS films and an increased utilization of Si island edges in CMOS/SOS circuits.

C. THE MEASUREMENT OF STRAIN INDUCED ANISOTROPY

The existence of stress and concomitant strain in thin oxide films grown on silicon wafers is well documented.[1,2] The elasto-optic properties of the oxide and the thermal expansion coefficient mismatch between the oxide and the silicon substrate have been used to estimate the optical anisotropy[11] induced in the oxide layer when the oxide cools after growth. Other workers observed anisotropy in the oxide[12] and an inner layer between the oxide and the substrate.[12,13] On the basis of our prior work[14] on the ellipsometric measurement of strain-induced anisotropy in optical film materials, we estimated the magnitude of the ellipsometric "errors" that would be generated in SiO_2 films grown on a silicon wafer. These ellipsometric "errors," or anisotropic shifts, were obtained by first calculating the Fresnel reflection coefficients[15] from an unstrained oxide film model and then calculating these coefficients for the strained or anisotropic film model. These complex reflection coefficients r_p and r_s, expressed as the ratios of their real and imaginary components R_p/R_s and $\exp(i\Delta_p)/\exp(i\Delta_s)$, are easily represented by two variables, ψ and Δ, which are directly measurable in an ellipsometer.[16] These two variables can be calculated for either a strained film or an unstrained film, and this "simulated" data can be processed in a conventional ellipsometer data processing program to obtain the film thickness and the refractive index. These "processed" film index and thickness values are then compared with the starting values to determine the degree of distortion introduced into the measurements by the presence of anisotropy.

These anisotropy simulation calculations predicted significant errors in the measurement of the refractive index of SiO_2 films on silicon at certain film thicknesses and angles of incidence. However, when a series of experimental measurements was completed on these films, anomalies were observed that in many cases were too large to be explained by the anisotropy

effect alone. In some cases, the Δ,ψ data processed in the computer would not yield an answer. The computer data processing model did not represent the anisotropic experiment accurately because it was based on a single layer isotropic film on an isotropic substrate which ignored the existence of the SiO_x inner layer[12,13] between the SiO_2 film and the Si substrate. The presence of this film produces significant measurement errors that mask the effect of anisotropy in the SiO_2 film.

The solution to this problem was to generate a new computer algorithm or method of data processing based on a multiple layer film structure with anisotropy in the film and the substrate. In using this method, the Δ,ψ data are taken as a function of the angle of incidence ϕ of the light on a multiple film sample and tabulated in the computer. The various fitting parameters, such as refractive index, anisotropy, and film thickness, are iterated until the optimum fit to the complete Δ,ψ,ϕ data set is obtained. The use of multiple angle data is necessary to resolve the various anisotropy and multiple-film effects. This method has proven to be very valuable not only for evaluating the anisotropy induced in the thin oxide film by stress but also for evaluating the refractive index and thickness of the SiO_x inner layer. It is the only method available that yields both types of data without using wide spectral range measurements.[13] The only limitations to the method are that the number of layers must be known (1, 2, or 3) and that the film thicknesses must lie in specific ranges for the anisotropy measurement to be very sensitive.

D. KEY RESULTS

The first objective of the proposed study was to develop an accurate and reproducible technique for measuring the interfacial stress in thermally oxidized Si and in epitaxial SOS. Hughes believed that the ellipsometric stress measurement technique was ideally suited for this purpose and therefore proposed its development and use in this program. The technique, described in detail in Section 2, is simple and straightforward to apply and has the advantages over mechanical measurement schemes of being non-destructive and non-contacting. It has an advantage over diffraction techniques in that it can measure noncrystalline films such as SiO_2.

The ellipsometric stress measurement technique utilizes the uniaxial anisotropy induced in a stressed thin film to determine the amount of stress acting at the film boundary. This technique has been developed exclusively at Hughes Research Laboratories. The technique is highly sensitive and had previously been used successfully to measure stress in films of As_2Se_3, As_2S_3, ZnSe, and ThF_4 on KCl substrates. A more complete description is presented in Section 2.A.

The ellipsometric stress measurement technique was found to be a very useful tool for measuring non-destructively the values of interfacial stress in both the Si/SiO_2 and SOS systems. However, each of these structural systems posed unique problems requiring modifications of existing techniques to obtain meaningful results from ellipsometric data. Section 2.B describes an important limitation on the sensitivity of the ellipsometric technique which restricts its use to certain thickness ranges when measuring anisotropy in thermal silicon oxides.

Films of silicon oxide, silicon nitride, and silicon-on-sapphire were prepared for use in this program as described in Section 2.C. Sections 2.D and 2.E present data obtained from ellipsometric measurements on the prepared oxide, nitride, and SOS samples.

Data evaluation and conclusions are summarized in Section 3. The usefulness of the ellipsometric technique for measuring stress in oxide and SOS films is evaluated in Section 3.A. Correlations of oxide stress with oxidation and anneal conditions are made in Section 3.B, while Section 3.C discusses the results of capacitance-voltage (C-V) measurements made on thermally oxidized samples. The stress observed in SOS wafers and its correlation with the manufacturer's quality grading system are discussed in Section 3.D.

Appendix A briefly describes the experimental technique used to make the multi-angle ellipsometric measurements. Appendices B and C present theoretical analyses of the effect of anisotropy in the refractive index of a film on its reflectance of polarized light and of the correlation between the anisotropy and the stress tensor in the film, respectively. Appendix D is a retrospective that indicates the evolution of our understanding of the optical behavior of strained, multilevel films and the

[illegible] complexity of the analytical tools required to interpret the [illegible] contained in the [illegible] reflectometer.

The key results obtained are summarized below. During this study [illegible]:

- Developed a technique measuring the optical properties of multilevel thin films using multi-angle ellipsometry. From the observed optical properties, information can be gained regarding the thickness and refractive index of each of the layers and the stresses existing in each of the film layers.

- Used this technique to confirm the existence of an inner layer between the oxide and silicon in the thermally grown Si/SiO_2 system. This layer is between 3.3 and 5.6 Å thick and has an index of refraction between [illegible] and [illegible].

- Observed compressive stress in thermally grown silicon oxides in a range from 8×10^8 to 2.5×10^9 dyn/cm^2, in good agreement with published values.[1,2,3]

- Measured large optical anisotropies in SOS [illegible] using the same ellipsometric technique. Compressive and shear stress components deduced from the [illegible] correlate strongly with SOS film quality as deduced by [illegible] inspection.

SECTION 2

ELLIPSOMETRIC TECHNIQUE AND RESULTS

A. FUNDAMENTAL ELLIPSOMETRY

An ellipsometer is often used to measure the reflection coefficients of substrates and films. When these substrates and films are isotropic, their reflection properties can be represented by an amplitude and a phase factor for the polarization state parallel to the plane of incidence and by a different amplitude and phase factor for the other polarization state (as shown in Figure 1). The polarization properties of the sample are thus encoded on the reflected light, these properties can be represented by the relative phase shift, $\Delta = \Delta_p - \Delta_s$ for the two polarizations and the ratio of the amplitude reflection coefficients, $\tan\Psi = R_p/R_s$. The angles Δ and Ψ thus represent the Fresnel reflection coefficients of the sample as shown in Figure 2 for both cases, and they can be measured in an ellipsometer by measuring the angular positions of several optical components.

In an ellipsometer, a schematic is shown in Figure 3 -- monochromatic linearly polarized light is passed through a quarter-wave plate oriented at 45° to the plane of incidence. It is well known that rotating the polarization vector at the input to the wave plate causes the output polarization to be resolved into two orthogonal equal-amplitude linear polarization vectors with a specific relative phase angle between them. The input polarizer adjusts the phase of these two orthogonal polarization vectors incident on the sample. If an appropriate setting of the polarizer is selected, then the relative phase shift of the two incident polarizations cancels the reflection phase shift Δ of the sample, and the reflected waves are in phase. This produces a linear resultant polarization vector that can be nulled by rotating the analyzer for minimum transmission. The angular position of the analyzer is orthogonal to the resultant polarization vector angle Ψ which is then the inverse tangent of R_p/R_s.

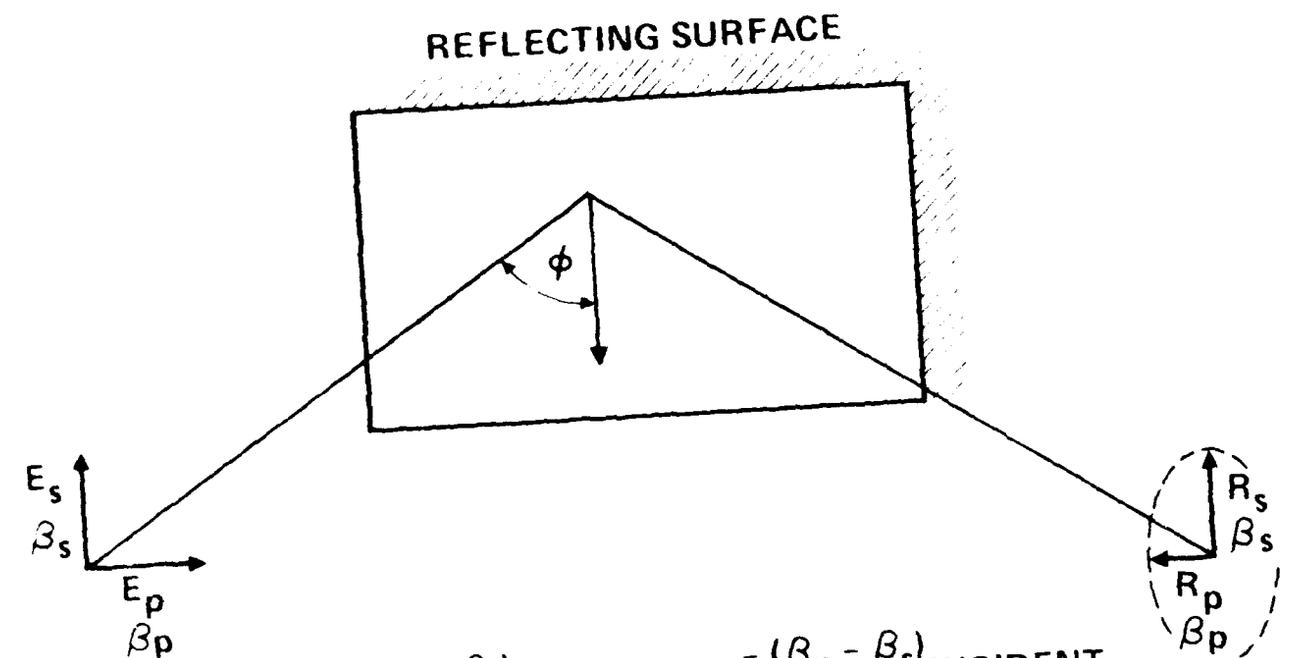

- $\Delta = (\beta_p - \beta_s)_{REFLECTED} - (\beta_p - \beta_s)_{INCIDENT}$
- $\psi = \arctan\left(\frac{R_p/E_p}{R_s/E_s}\right)$

$= \arctan\left(\frac{R_p}{R_s}\right)$ FOR $E_p = E_s$

Figure 1. Ellipsometry technique

- $r = R^1 E^1 = (R/E)\, e^{i\beta}$

- $r_{12}^{p} = \dfrac{n_1 \cos \phi_2 - n_2 \cos \phi_1}{n_1 \cos \phi_2 + n_2 \cos \phi_1}$,

- $r_{12}^{s} = \dfrac{n_1 \cos \phi_1 - n_2 \cos \phi_2}{n_1 \cos \phi_1 + n_2 \cos \phi_2}$

- $\dfrac{r_p}{r_s} = \dfrac{R_p}{R_s} \cdot \dfrac{E_s}{E_p}\, e^{i(\beta_p - \beta_s)}$

- $\dfrac{r_p}{r_s} = \tan \Psi\, e^{i\Delta}$

- $n^2 - k^2 = t^2 \dfrac{(\cos^2 2\bar{\Psi} - \sin^2 2\bar{\Psi} \sin^2 \bar{\Delta})}{(1 + \sin 2\bar{\Psi} \cos \bar{\Delta})^2} + \sin^2 \phi$,

$$2nk = t^2 \frac{\sin 4\bar{\Psi} \sin \bar{\Delta}}{(1 + \sin 2\bar{\Psi} \cos \bar{\Delta})^2},$$

t sin ‡ tan ¢

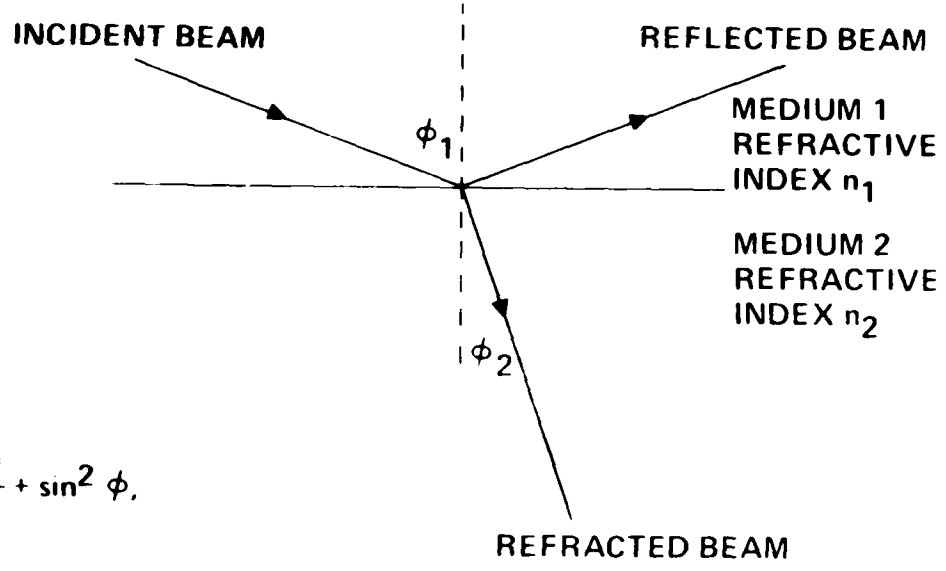

Figure 2. The Fresnel coefficients of a substrate.

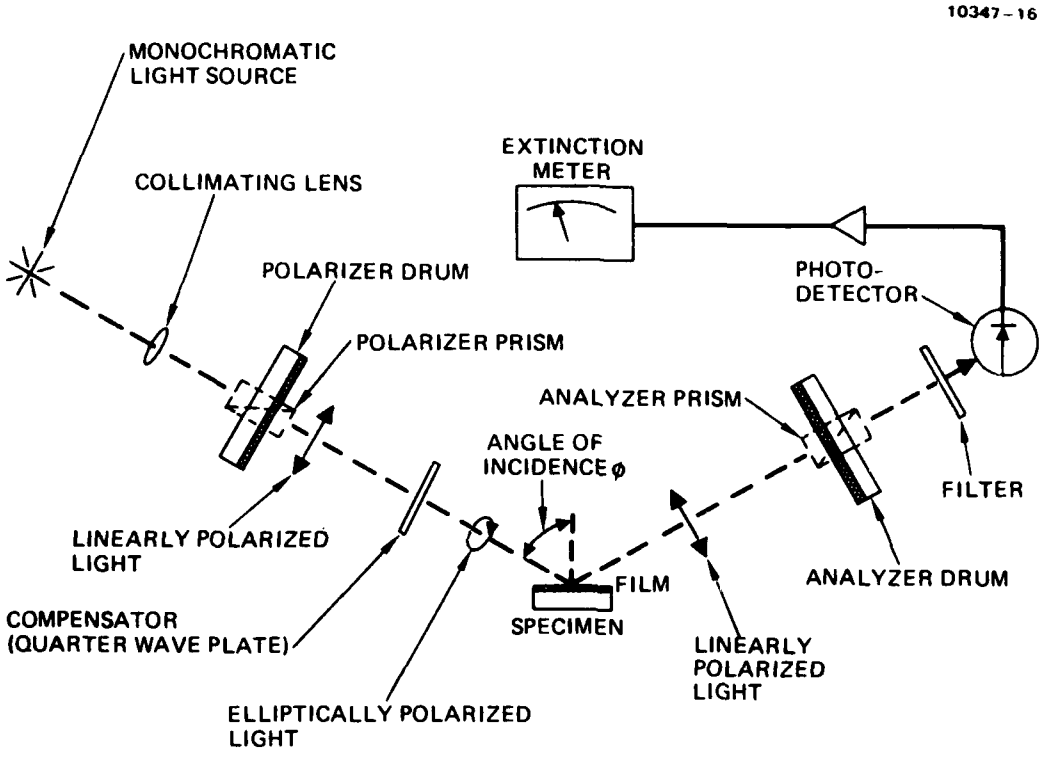

Figure 3. Schematic of an ellipsometer.

Thus in the nulling type of ellipsometer, the operator measures the "parameters" Δ and ψ by alternately adjusting the input polarizer and the output analyzer until a null reading occurs in a meter, as shown in Figure 3. The angular positions of the polarizer and analyzer are then recorded and processed in simple algebraic equations to derive Δ and ψ. These parameters and the angle of incidence ϕ are then fed into a data-processing program which calculates the Fresnel coefficient ratio (ρ) as a function of substrate index or as a function of the refractive index and thickness of the thin film. The program iteratively evaluates the properties of a sample by finding the best index or the best index and thickness to fit the experimental values of ψ, Δ, and ϕ. This technique is capable of measuring films as thin as a few angstroms or as large as several micrometers with great accuracy. However, if the samples are anisotropic or multilayered, the data evaluation process is complex, and measurements made at a single angle of incidence may not provide sufficient data to unambiguously evaluate the layers. In Appendix A, we outline the procedure for making ellipsometric measurements under these conditions.

When the sample under investigation contains more than a single film layer or when it is anisotropic or both, the measured ellipsometric parameters at a single angle of incidence provide no clues as to the existence of anisotropy or multiple layers in the films. When these parameters are processed in the computer, they yield index and thickness values for a hypothetical single-layered isotropic film. It is clear that one ellipsometric measurement provides a set of Δ, ψ, and ϕ data, and the single anisotropic film requires at least four data — N, ΔN, K, and T — to describe it completely. In the case of a layered film system, four or more data are needed to describe each layer. It is obvious that the ellipsometric data can be increased by taking data at several angles of incidence (ϕ_1, ϕ_2, ϕ_3, etc.). The problem is how to use this additional data to evaluate the layers.

Our approach has been to generate a theoretical model of the multiple-layered film structure that allows for the substrate and each film layer to be anisotropic and to have real and imaginary refractive index components. With this model, tables of theoretical values of Δ and ψ versus ϕ can be generated for various values of film parameters.

least-squares error program is used to compare the theoretical Δ, ψ, ϕ data tables with the experimental Δ, ψ, ϕ data tables and to select the set with the least error. Because many calculations are involved in the "match up" process, this program was made semi-automatic, and the computer operator defined the parameter search range for the iterative data analysis. In this multiple-angle ellipsometric method, the computer operator must also know the number of layers in the film being evaluated. Thus, the operator selects ranges of film thickness, real and imaginary index, and index anisotropy for each film layer, and ranges of real and imaginary index and anisotropy for the substrate. Using these initial parameter search ranges, a first best fit is found and the least-squares error values for Δ and ψ are displayed. The operator can then iterate on any two parameters to obtain a better second fit, third fit, etc. until the lowest minimum is obtained. This technique has been successfully applied at HRL to the evaluation of a wide variety of thin-film systems.

B. THEORETICAL SENSITIVITY OF THE METHOD

We have analyzed the sensitivity of the multiple-angle ellipsometry technique for measuring anisotropy in films of varying thickness. The analysis entails calculating theoretical tables of Δ and ψ as a function of the angle of incidence ϕ for a specific anisotropic film structure and then processing these data in the multiple-angle ellipsometric data processing program to obtain the best parameter fit <u>without</u> using anisotropy. In effect, we start with specific substrate and film refractive indices, film anisotropy, and film thickness values and generate a perfect set of Δ, ψ versus ϕ data in an anisotropic computer simulation program. Then these data are analyzed in <u>another</u> computer data processing program which finds the optimum fit to the Δ, ψ data by varying the film thickness, the film index, and the substrate index. In the latter analysis, the anisotropy is assumed to be zero and this leads to convergence errors in Δ and ψ. The size of these convergence errors is a measure of the sensitivity of this multiple angle ellipsometric technique for detecting anisotropy in thin films. When this simulation process is performed as

a function of film thickness for a single value of anisotropy, the convergence error "results" allow us to predict those film thickness regimes that are the best choice for measuring anisotropy, and therefore stress, in films.

The results of these calculations for SiO_2 films on silicon are given in Figure 4. In these calculations, an anisotropy of 0.001 was assumed for the SiO_2 layer, and no anisotropy was permitted in the data-fitting process. An inner layer thickness of 6 Å and a refractive index of 2.6 were also used. The refractive index of the substrate was taken to be 3.8714 - i0.025, and the refractive index of the oxide film was 1.457. The results are presented as the convergence error in Δ and the convergence error in ψ. It is apparent that the convergence error in Δ is much larger than the convergence error in ψ over much of the film thickness range. This means that the presence of anisotropy in the film has a stronger effect on Δ than on ψ and that errors in determining Δ will have a larger effect on the accuracy of the anisotropy measurement than will errors in determining ψ. Also shown in Figure 4 is a horizontal dashed line at the Δ,ψ convergence level of 0.05°. This represents the experimental error in measuring Δ and ψ. It is immediately obvious that film thicknesses below 4000 Å will not be useful for measuring anisotropy because the convergence drive error in Δ is less than or equal to measurement error, i.e., the signal-to-noise ratio is poor. Above 4000 Å, there are specific narrow film thickness regions where the convergence drive Δ error signal is larger than the Δ measurement error signal. These are regions where the anisotropy can be measured with good convergence and high accuracy. The method is not inaccurate at 4,000 Å, but it is marginal at 4,300 Å. The first "good" anisotropy measurement region occurs at 7,000 Å, where the ratio of the convergence error to the measurement error is about 4 to 1. The best anisotropy measurement region that we have found occurs between 11,500 Å and 12,000 Å and it has an error ratio of about 11 to 1. We expect that the technique will be more accurate with thicker films because the optical path anisotropic phase shift will be higher. In Figure 4, the peaks in the theoretical curve show a monotonic increase in Δ convergence drive with film thickness, which supports this hypothesis.

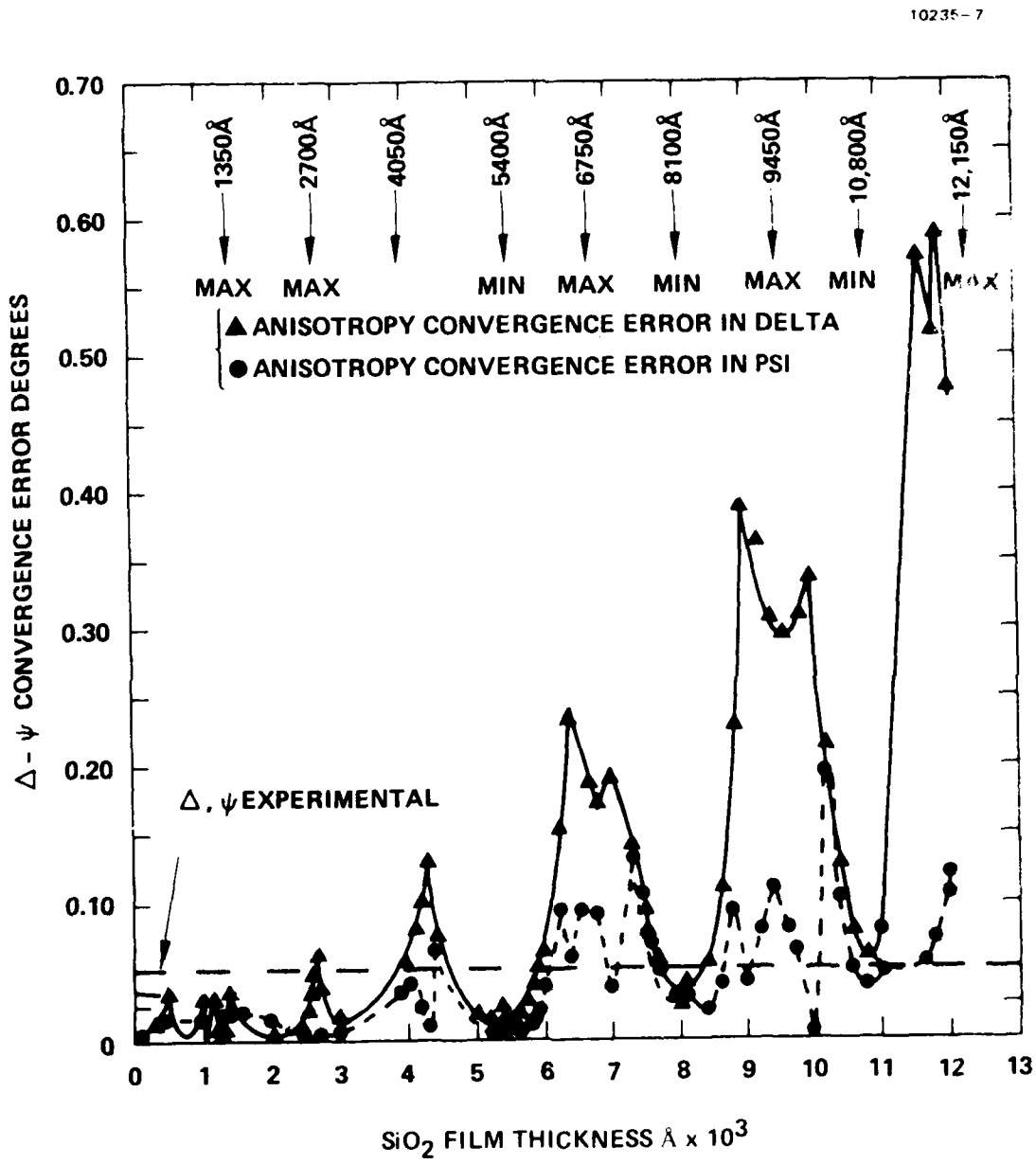

Figure 4. Anisotropy measurement sensitivity versus film thickness for SiO_2 on Si.

Although the Δ convergence error plays the strongest role in measuring the anisotropy, the ψ convergence error cannot be ignored because it strongly affects the measurement accuracy of the other film parameters and of the inner layer parameters. Failure to determine these parameters accurately will affect the anisotropy accuracy.

C. MATERIALS PREPARATION

1. Oxide on Silicon

During the preparation of thermally oxidized silicon samples, growth and anneal conditions were varied to obtain samples with differing amounts of stress in the oxide. Table 1 shows the conditions under which each wafer was prepared and the measured thicknesses of the resulting oxides. In this table, "dry" refers to oxidation in O_2 ambient, while "wet" refers to an ambient consisting of premixed O_2 and H_2 gases. A "quenched" sample was cooled at a rate estimated at 2000°C/min, while "unquenched" samples saw a cooling rate of 200°C/min. All anneal cycles were performed after the samples had cooled to room temperature, and all were slow-pulled (unquenched). Table 2 lists the general preparation sequence for all lots.

In an effort to bring the oxide thicknesses into ranges where stress could be measured most reliably (see Section 2.B), lot STF-3 was partially etched back after completion of the growth cycle until an appropriate oxide thickness was obtained. These wafers are designated in Table 1 as STF-3E-1A, -1B, -2A, and -2B.

Completed wafer lots were delivered for ellipsometric evaluation or C-V measurement as appropriate. The results of the ellipsometric study are reported in Section 2.D, and the C-V results are discussed in Section 3.C.

2. Nitride on Silicon

A sample of a silicon nitride film deposited on silicon was obtained from the Hughes Newport Beach Research Center for evaluation using the ellipsometric stress measurement technique. This film was deposited in a standard CVD nitride deposition system which employs the nitridation of silane in ammonia ambient at 875°C. The nitride was deposited to a thickness of 925 Å.

Table 1. Oxidation and Anneal Conditions for Oxide Stress Samples

Wafer	Type	Oxidation Conditions				Anneal Conditions		Thickness
		Temp, °C	Time, min	Wet/Dry	Quench	Temp, °C	Time, min	
STF-3 -1A	p	1100	420	W	Y	925	15	11,820
STF-3 -1B	p	1100	420	W	Y	—	—	11,850
STF-3 -2A	p	1100	420	W	Y	925	30	11,680
STF-3 -2B	p	1100	420	W	Y	—	—	11,720
STF-3E-1A	p	1100	420	W	Y	925	15	8,090
STF-3E-1B	p	1100	420	W	Y	—	—	8,090
STF-3E-2A	p	1100	420	W	Y	925	30	7,950
STF-3E-2B	p	1100	420	W	Y	—	—	7,940
STF-11- 1	n	1100	11.5	W	Y	—	—	1,450
STF-11- 2	n	1100	11.5	W	Y	925	30	1,490
STF-11- 5	n	1100	11.5	W	N	—	—	1,440
STF-11- 6	n	1100	11.5	W	N	925	30	1,460
STF-11- 9	n	1000	35	W	Y	—	—	1,450
STF-11-10	n	1000	35	W	Y	925	30	1,440
STF-11-13	n	1000	35	W	N	—	—	1,510
STF-11-14	n	1000	35	W	N	925	30	1,520
STF-11-17	n	925	109	W	Y	—	—	1,540
STF-11-18	n	925	109	W	Y	925	30	1,560
STF-11-21	n	925	109	W	N	—	—	1,610
STF-11-22	n	925	109	W	N	925	30	1,600
STF-12- 1	n	1100	32	W	Y	1000	30	2,940
STF-12- 2	n	1100	32	W	Y	—	—	2,900
STF-12- 3	n	1000	97	W	Y	1000	30	2,790
STF-12- 4	n	1000	97	W	Y	—	—	2,770
STF-13	n	1100	210	D	Y	—	—	2,810
STF-14- 2	p	1100	210	D	Y	1000	30	2,470
STF-14- 4	p	1100	210	D	Y	1000	60	2,530
STF-14- 6	p	1100	210	D	Y	925	60	2,430
STF-14- 8	p	1100	210	D	Y	925	120	2,600
STF-14-10	p	1100	210	D	Y	—	—	2,520
STF-15- A	n	1100	26	W	Y	—	—	2,450
STF-15- C	n	1100	139	W	Y	—	—	6,540
STF-15- E	n	1100	261	W	Y	—	—	9,130
STF-15- G	n	—	—	—	—	—	—	100

Table 2. Preparation Sequence for Oxide Stress Samples

Pre-furnace clean	
Oxidation	(see Table 1 for specific conditions)
Cool	
Anneal	(see Table 1 for specific conditions)
Cool	
Film thickness measurement (Nanospec)	

3. Silicon-on-Sapphire

Preliminary ellipsometric stress measurements were made on a 2-in., 0.5-μm-thick SOS wafer designated SOS-II. This wafer was taken from an SOS lot of device quality wafers obtained from Union Carbide.

Subsequently, 3-in., 0.5-μm-thick SOS samples were also obtained from Union Carbide for study in this phase of the stress program. These SOS wafers were selected by Union Carbide to represent their four grades of material quality as determined by optical reflectance measurements. These samples were given wafer IDs SOS-10, -11, -12, and -13. The correspondence between wafer ID and Union Carbide quality grade is shown in Table 3. Ellipsometric stress measurements were made on these samples as received; these results are reported in Section 2.E.

Table 3. Wafer Identification for SOS Samples

Sample	Quality Grade (Union Carbide)
SOS-10	No haze
SOS-11	Light haze
SOS-12	Medium haze
SOS-13	Very light haze

D. EXPERIMENTAL RESULTS — SILICON DIOXIDE ON SILICON

To test the theoretical predictions of the anisotropy simulation studies, several SiO_2 film experiments were performed over a variety of oxide film thicknesses ranging from 1,500 to 11,800 Å. Those experiments that yielded the most significant results are reported here. In brief, anisotropy was observed in samples having film thicknesses near 6500 Å, 9000 Å, and 11,800 Å. Other film thicknesses did not yield reliable anisotropic results, in agreement with theoretical predictions. The presence of a transition layer between the oxide and the silicon played a major role in interpreting the ellipsometric data.

1. Strain Annealing Experiment — 11,800 Å Film Thickness

A controlled oxide annealing experiment was designed and executed on the basis of the theoretical study, which predicted significant sensitivity for anisotropy at specific film thickness values. In this experiment, wafer lot STF-3, consisting of two wafers designated STF-3-1 and STF-3-2, were placed in an oxide furnace and processed at 1100°C to produce 11,800-Å-thick oxide films. The wafers were withdrawn slowly from the furnace to minimize stress in the oxide films. Next, the wafers were scribed and then broken into two halves labeled A and B. The A samples were annealed at 925°C for two different times: sample STF-3-1A for 15 min and sample STF-3-2A for 30 min. The results of the ellipsometric measurements on these four samples, given in Table 4, clearly show that annealing reduces the stress in the oxide layers and by so doing reduces the measured optical anisotropy in the films. Specifically, the longer annealing time for sample STF-3-2A resulted in a lower stress value for it than for STF-3-1A.

These results, which include the measurement of stress levels ranging from 1.4×10^9 dyn/cm^2 to 2.5×10^9 dyn/cm^2 in SiO_2 films are the first direct measurements of anisotropy and stress in oxide films ever obtained by ellipsometry.

An important side benefit of this experiment is the evaluation of the refractive index and thickness of the SiO_2 inner layer which exists

Table 4. Multiple Angle Ellipsometric Analysis of Stressed and Annealed Oxide Layers on Silicon

Sample Identification	Data Fitting Δ Error, Deg	ψ Error, Deg	Film #1 Thickness, (T_1) Å	Film #1 Index (N_1)	Film #1 Anisotropy ΔN_1	Film #2 Thickness, (T_2) Å	Film #2 Index (N_2)	Film #1 Stress (σ), Dynes/cm^2	Sample Condition Code Oxidation, Annealed
STF-3-1A	0.16	0.16	11822	1.4607	-0.00071	5	2.16	-1.994×10^9	B-1
STF-3-1B	0.19	0.19	11850	1.4600	-0.00088	5	2.4	-2.472×10^9	B-0
STF-3-2A	0.17	0.17	11680	1.4621	-0.00051	3	2.8	-1.433×10^9	B-2
STF-3-2B	0.046	0.027	11720	1.460	-0.00090	4	2.6	-2.528×10^9	B-0

OXIDATION CODE

A	Wet, 1000°C Pulled Fast
B	Wet, 1100°C Pulled Slowly
C	Wet, 1100°C Pulled Fast
D	Dry, 1100°C Pulled Fast

ANNEALING CODE

1	925°C, 15 min
2	925°C, 30 min
3	925°C, 60 min
4	925°C, 120 min
5	1000°C, 30 min
6	1000°C, 60 min
0	No Anneal

between the silicon and the SiO_2 layer. If the existence of this layer is ignored in the data analysis process, then large errors will occur in fitting the data with the result that the optical anisotropy cannot be evaluated. Thus, the appropriate values for the inner layer thickness and index are evaluated by iteration in a least-squares data-processing algorithm, and then the value of the anisotropy is obtained by the same process. Repeated iteration over all of the parameters is necessary to obtain the optimum convergence solutions tabulated here. The strain in sample STF-3-1A was reduced by 20% as compared to sample STF-3-1B by a 15-min anneal at 925°C. The strain in sample STF-3-2A was reduced by 43% as compared to sample STF-3-2B by a 30-min anneal at 925°C. In this case at least, the annealing effect is roughly proportional to the annealing time.

2. Sample Etching Study

The curves presented in Figure 4 clearly show that anisotropy in an 8000-Å film would be difficult to measure because of the poor convergence error drive level. To test this hypothesis, the samples used in the annealing experiment were etched down to 8000 Å and labeled STF-3E-1A, -1B, -2A, and -2B (the E signifies etching). Since the stress conditions in the sample arise from thermal expansion coefficient mismatch effects at the interface, we assumed that the etching process could not alter the anisotropy in the SiO_2 film.

The results of measurements made on this set of etched samples is given in Table 5. As theoretically predicted, these films showed anisotropies that were either 0 or at most 1/20 those of the unetched samples, and the sign of the anisotropy was ambiguous. The ψ convergence error curve in Figure 4 is also small at a thickness of 8000 Å and should lead to errors in convergence of the inner layer and top layer parameters. Under this condition, several sets of values can be obtained for the film parameters with approximately the same convergence error. Thus, this film thickness regime is a poor choice for evaluating the anisotropic properties of films using multiple-angle ellipsometric methods.

Table 5. Multiple Angle Ellipsometric Analysis of Etched Oxide Layers on Silicon

Sample Identification	Data Fitting Δ Error, Deg	ψ Error, Deg	Film #1 Thickness, (T_1) Å	Film #1 Index (N_1)	Film #1 Anisotropy ΔN_1	Film #2 Thickness, (T_2) Å	Film #2 Index (N_2)	Film #1 Stress (σ) Dynes/cm^2	Sample Condition Code Oxidation, Annealed	
STF-3E-1A	0.22	0.030	8090	1.4577	-0.000031	6	3.09	-8.71×10^7	B-1	Etched Once
STF-3E-1B	0.075	0.027	8090	1.4586	0 ±0.000002	5	2.88	0 $\pm 5.62 \times 10^6$	B-0	Etched Once
STF-3E-2A	0.140	0.099	7950	1.4576	0	5	2.80	0	B-2	Etched Once
STF-3E-2B	0.145	0.098	7940	1.4585	0	5	2.80	0	B-0	Etched Once

OXIDATION CODE

A	Wet, 1000°C Pulled Fast
B	Wet, 1100°C Pulled Slowly
C	Wet, 1100°C Pulled Fast
D	Dry, 1100°C Pulled Fast

ANNEALING CODE

1	925°C, 15 min
2	925°C, 30 min
3	925°C, 60 min
4	925°C, 120 min
5	1000°C, 30 min
6	1000°C, 60 min
0	No Anneal

This result verifies the theoretical predictions of high accuracy in measuring anisotropy at some film thicknesses and low accuracy at other film thicknesses. It also provides us with some guidelines for picking the optimum film thickness for evaluating the anisotropy or the inner layer properties. The optimum film thickness may not be the same for both purposes.

3. Δ, ψ Parameter Studies

These multiple-angle ellipsometric studies produced Fresnel reflection coefficient data in the form of the ellipsometric parameters Δ and ψ. It is instructive to calculate the changes in Δ and ψ that occur in an oxide sample when it is annealed. Figure 5 shows the effect of annealing sample STF-3-1B to get sample 1A. The change in Δ is as large as 4.5° at an angle of incidence of 55°. The change in ψ is on the order of 1° at 55°. Similarly in Figure 6, the change in Δ is on the order of 4.5°, and the change in ψ is on the order of 0.75° for sample STF-3-2B annealed to get sample 2A. These changes in the parameters Δ,ψ are gross compared to the 0.05° measurement accuracy of the ellipsometer. This observed $\Delta(\Delta)$, $\Delta(\psi)$ effect is not entirely attributable to the annealing of stress in the samples because (1) the thicknesses of the oxide layers (SiO_2) in these samples were slightly different and (2) of annealing and partially because they correspond to different locations on the same wafers. The thickness data are given in Table 4. To relate these changes directly to anisotropy, the same sample (not two halves) would have to be measured in exactly the same position both before and after annealing. This would require precision sample indexing equipment. However, these results on two independent samples corroborate the effect of a large change in Δ with sample annealing. Similar sets of curves plotted in Figures 7 and 8 for the 8000 Å etched samples show changes in Δ and ψ that are less pronounced. These results correlate with the curve in Figure 4, which shows very little error in Δ and ψ when anisotropic data are analyzed with an isotropic model. This reinforces the theoretical argument that strain-induced anisotropy has a more observable effect at some film thicknesses than at others and has a larger effect on Δ than on ψ.

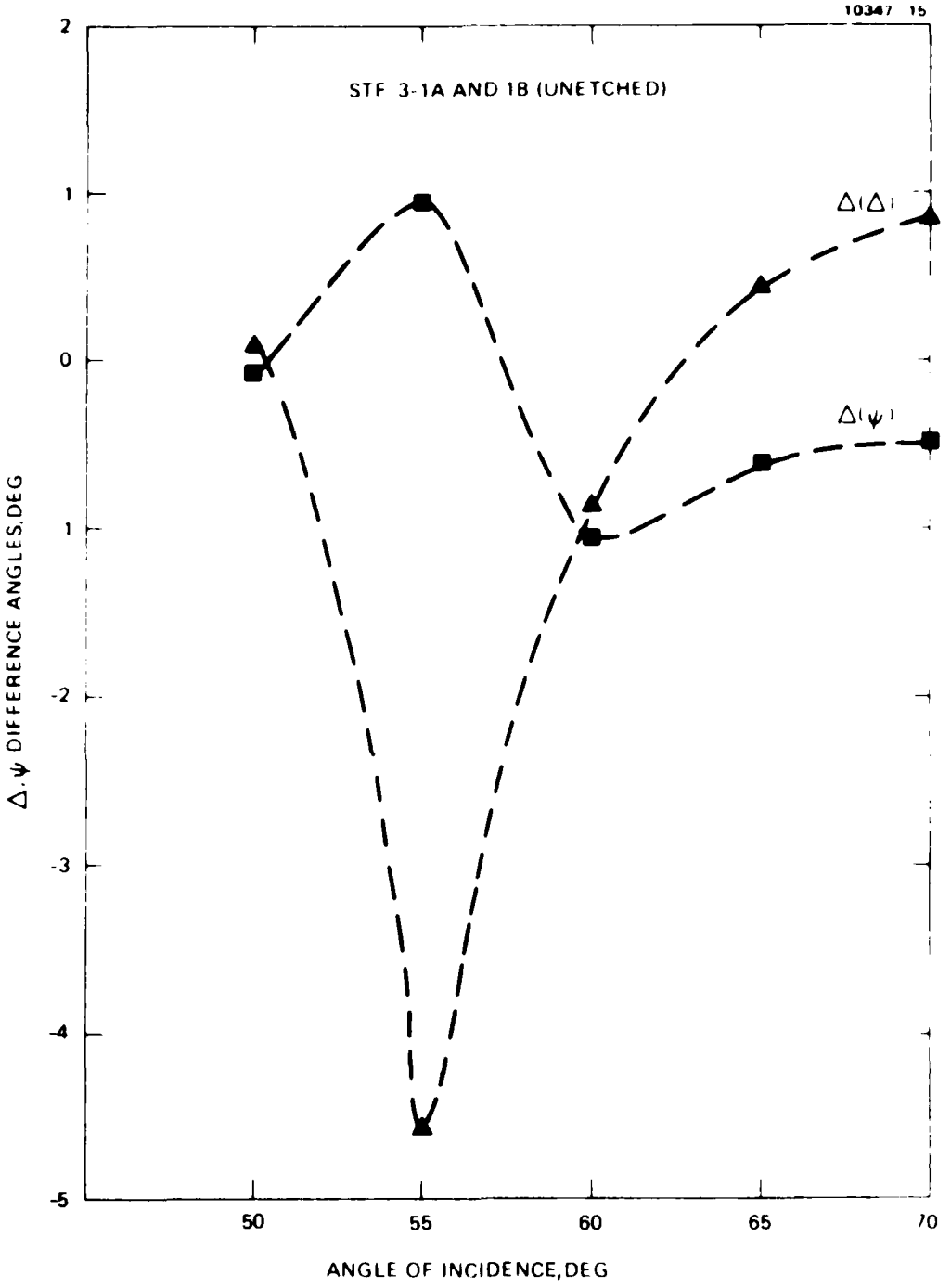

Figure 5. Ellipsometric Δ-ψ parameter changes due to sample annealing.

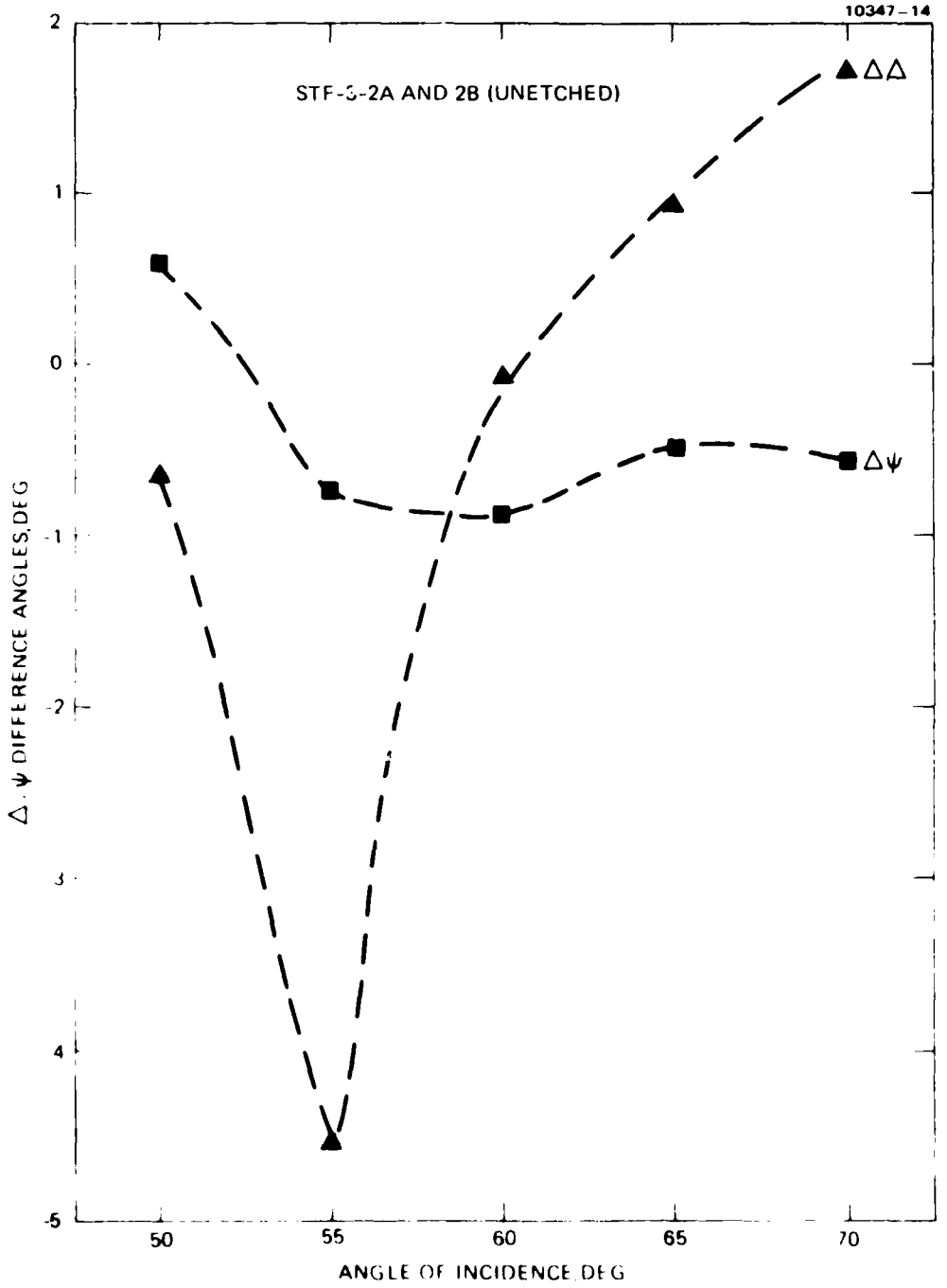

Figure 6. Ellipsometric parameter changes due to sample annealing.

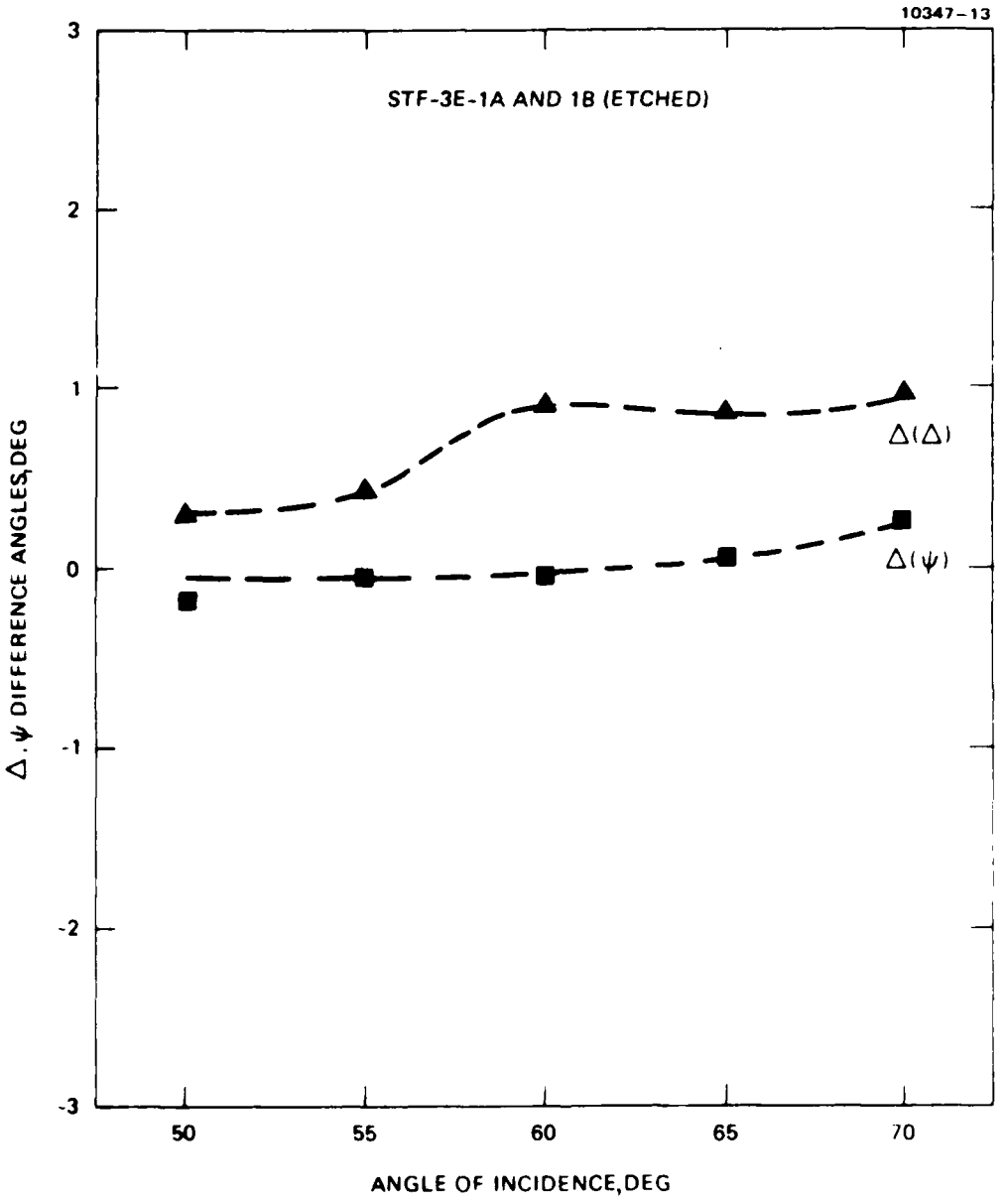

Figure 7. Ellipsometric parameter changes due to sample annealing.

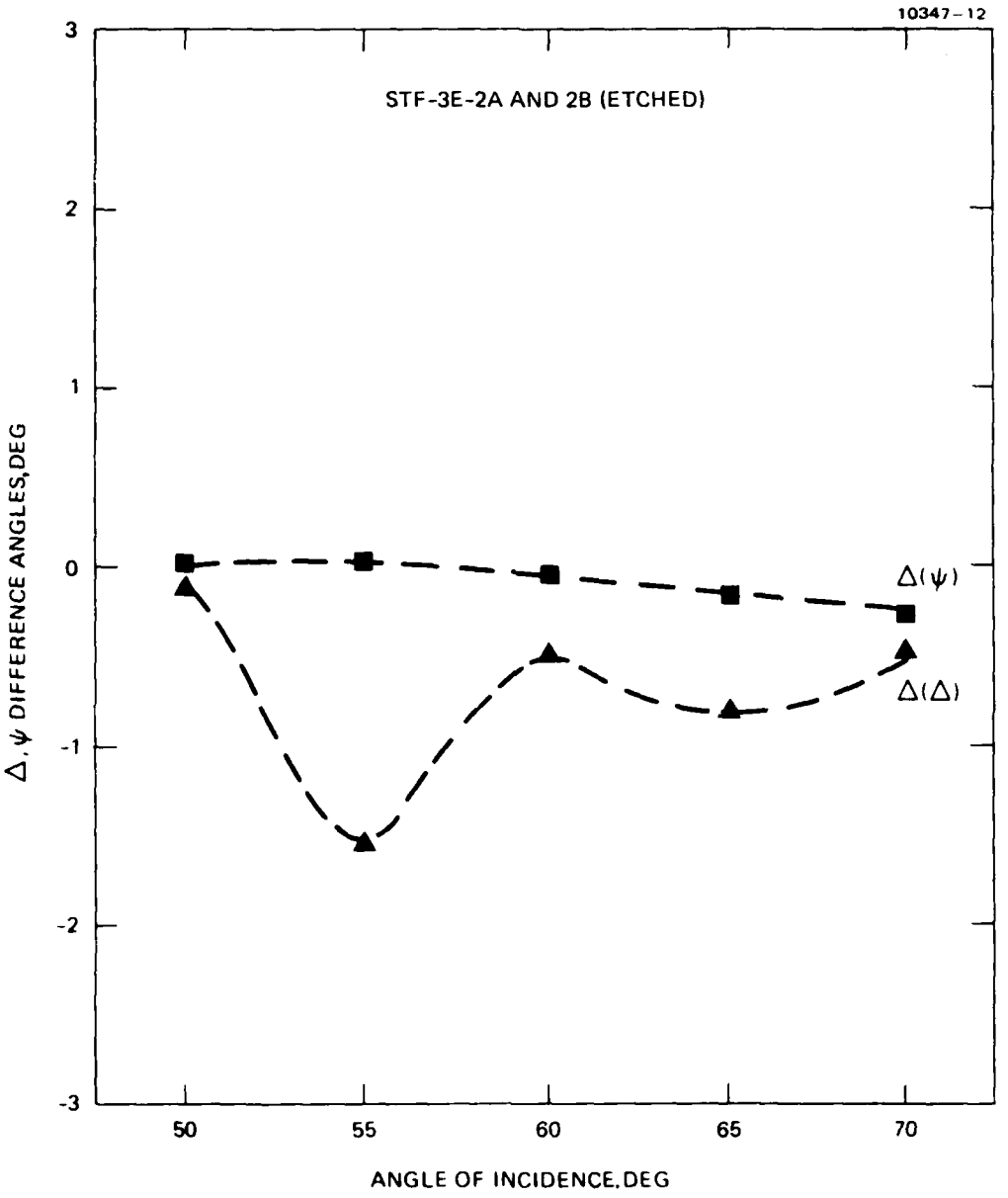

Figure 8. Ellipsometric Δ-ψ parameter changes due to sample annealing.

For completeness, we took the experimental Δ , ψ data for samples STF-3-1A and -1B and STF-3E-1A and -1B and processed them in a standard single-layer ellipsometer program. The results are given in Figures 9 through 12. The measured refractive indices increase very slightly with angle for the 11,800 Å thickness range films in Figures 9 and 10. For the etched 8000 Å thickness range films, the measured index values show a large anomaly at 60°. The dashed curves in Figures 9 through 12 were generated from the best data obtained from the multiple-angle data-fitting routine. The agreement here between experiment and theory is very good. The refractive index anomalies in Figures 11 and 12 are attributed to the presence of the SiO_x inner layer rather than to anisotropy because the theoretical curve can be generated without anisotropy.

4. Anisotropy in 6500 Å and 9000 Å SiO_2 Films

In Figure 4, the sensitivity of measuring anisotropy in SiO_2 films shows useful maxima at film thicknesses of 6500 Å, 9000 Å, and 11,800 Å. The results of the annealing experiments conducted at film thicknesses near 11,800 Å are presented above. This section presents the results of anisotropic measurements in the other two ranges of oxide film thickness. The results are given in Table 6. Film STF-15-E with a film thickness of 9130 Å shows an anisotropy of -0.00051, an inner layer thickness of 3 Å, and an index of 2.8. Sample STF-15-C with a film thickness of 6540 Å shows an anisotropy of -0.00030, an inner layer thickness of 0.5 Å, and an index 3.0. Below this result, the effect of neglecting the inner layer and anisotropy are shown. Since these films were processed for different growth periods at different times, they may have different anisotropy values due to different stress levels in each film. We suspect that the anisotropy in these films is more complicated than suggested by our perpendicular anisotropy model. When we aligned the sample tilt with crossed polarizer and analyzer in the ellipsometer, the optical null that we observed was an order of magnitude higher than that usually observed in thinner oxide films. This could be attributed to stress gradients in the films. Such gradients are not included in our simple anisotropy model,

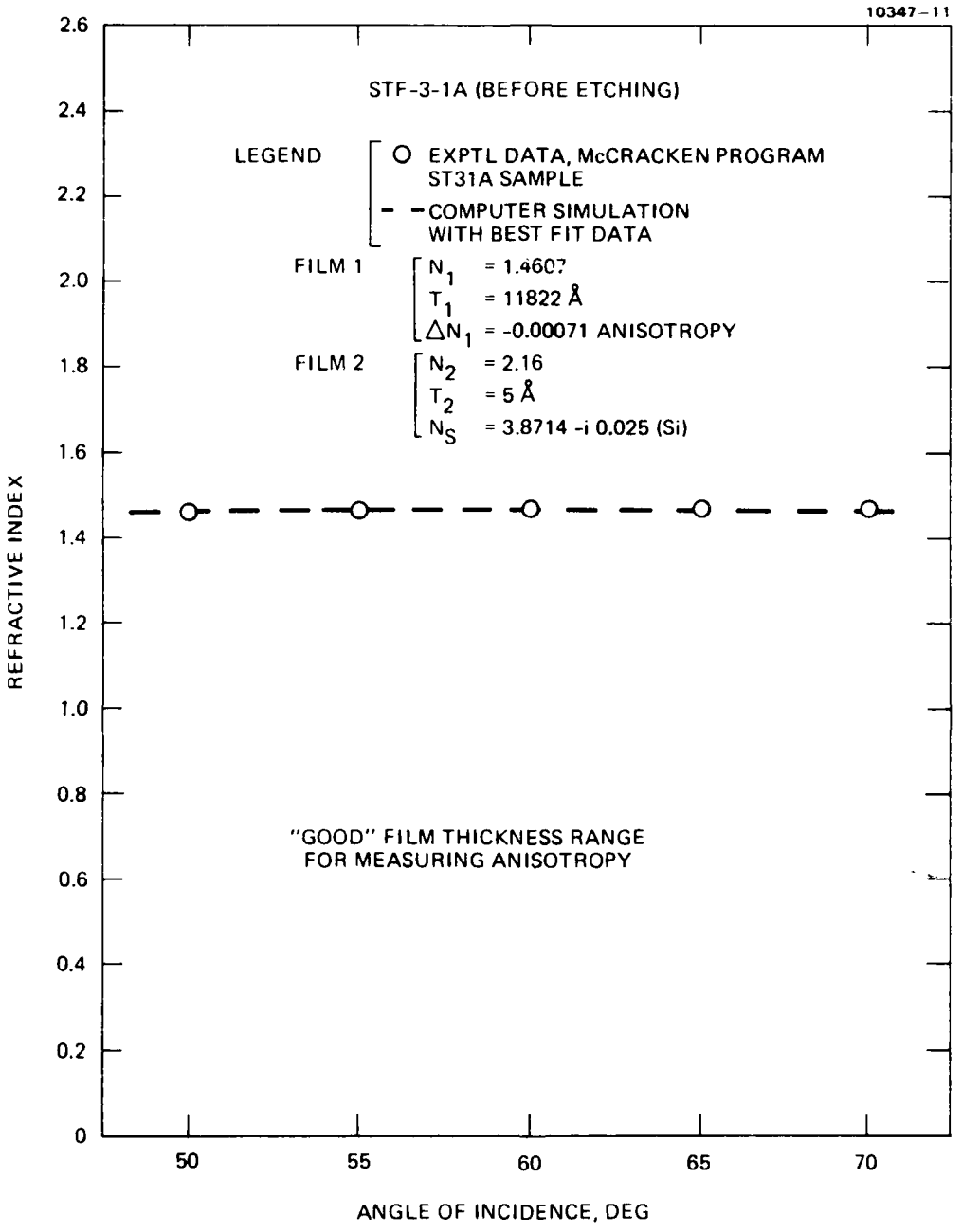

Figure 9. Refractive index versus angle annealed film SiO_2 on Si "good" film thickness range for measuring anisotropy.

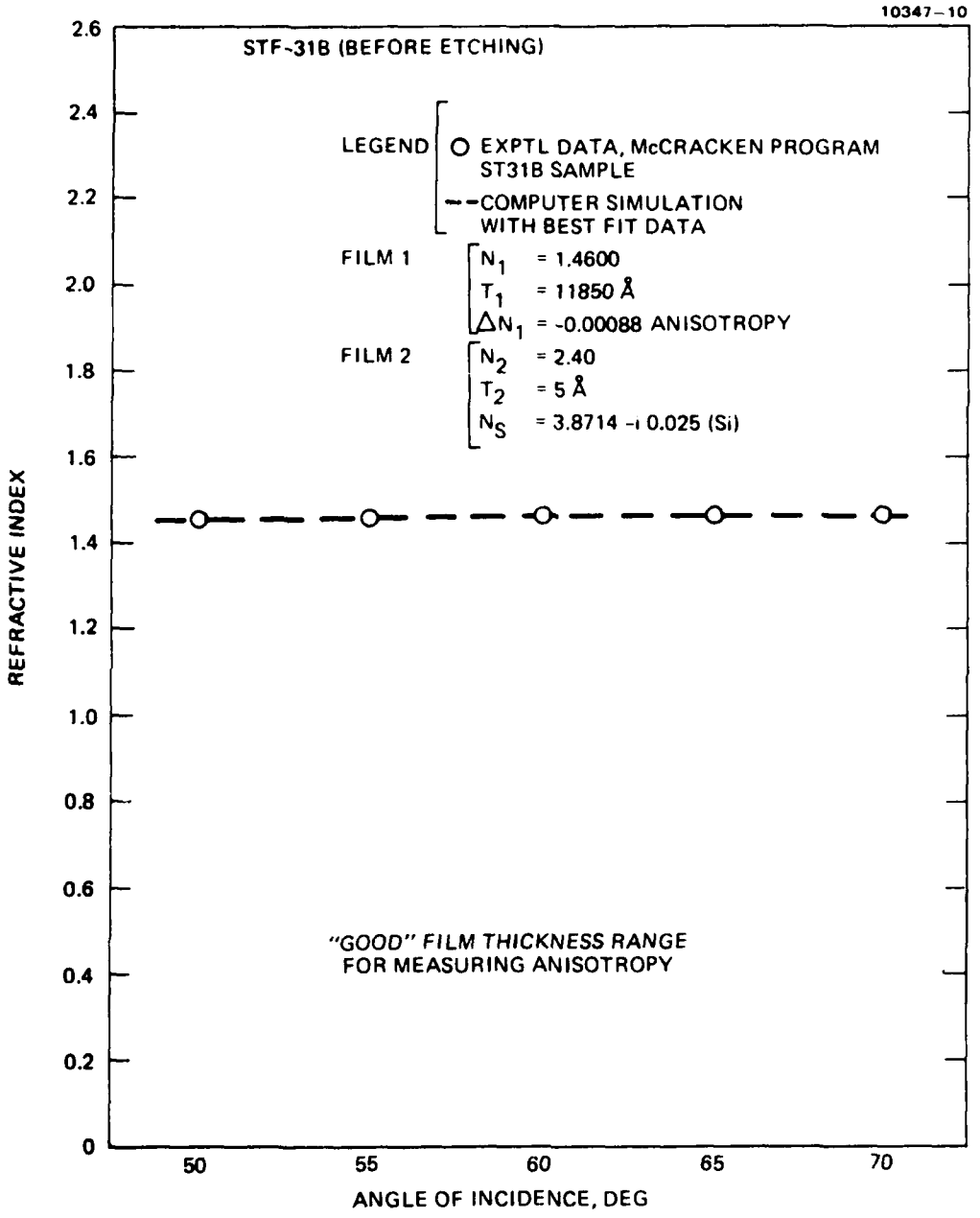

Figure 10. Refractive index versus angle unannealed film SiO_2 on Si "good" film thickness range for measuring anisotropy.

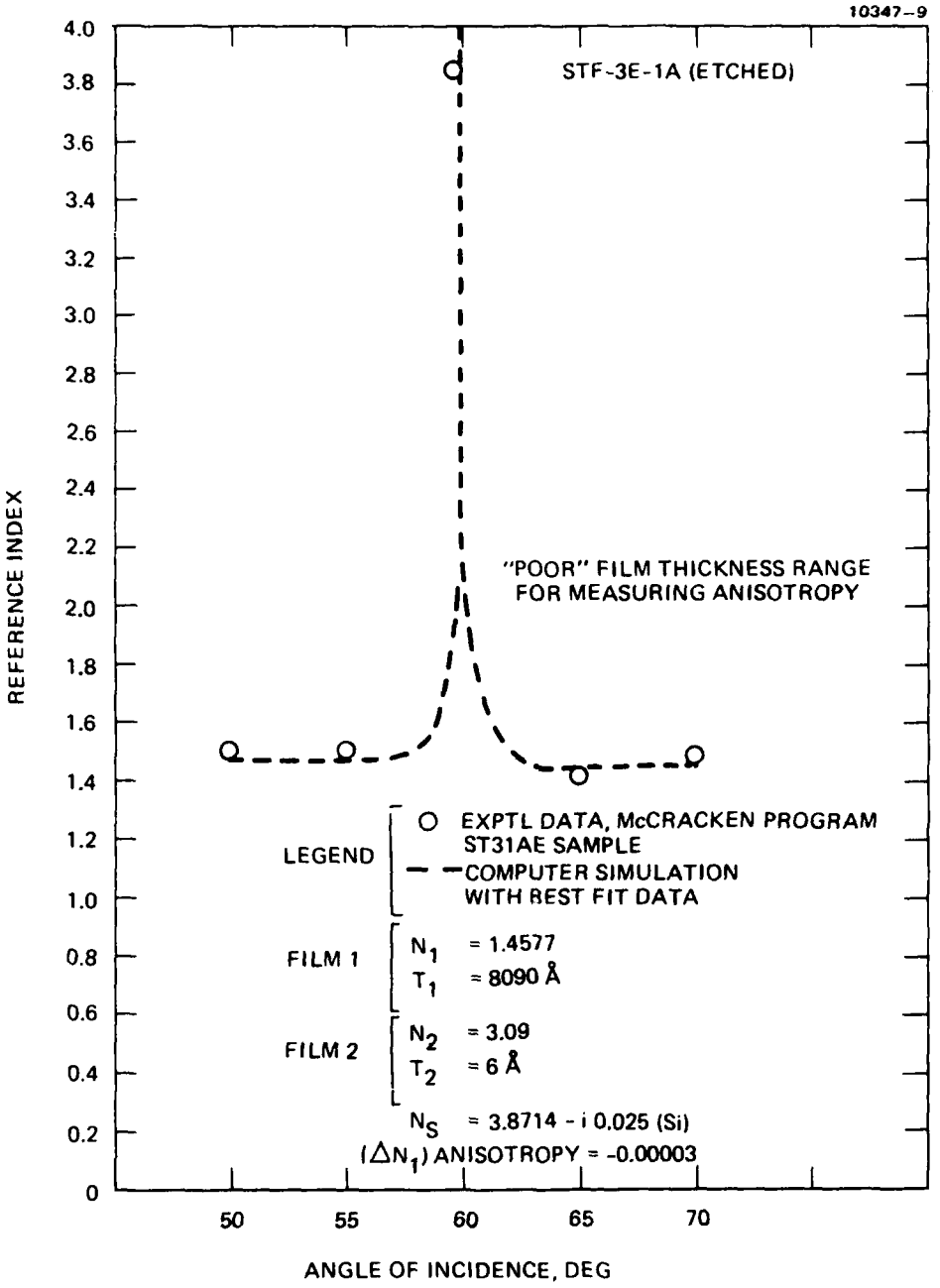

Figure 11. Refractive index versus angle annealed film SiO_2 on Si poor film thickness range for measuring anisotropy.

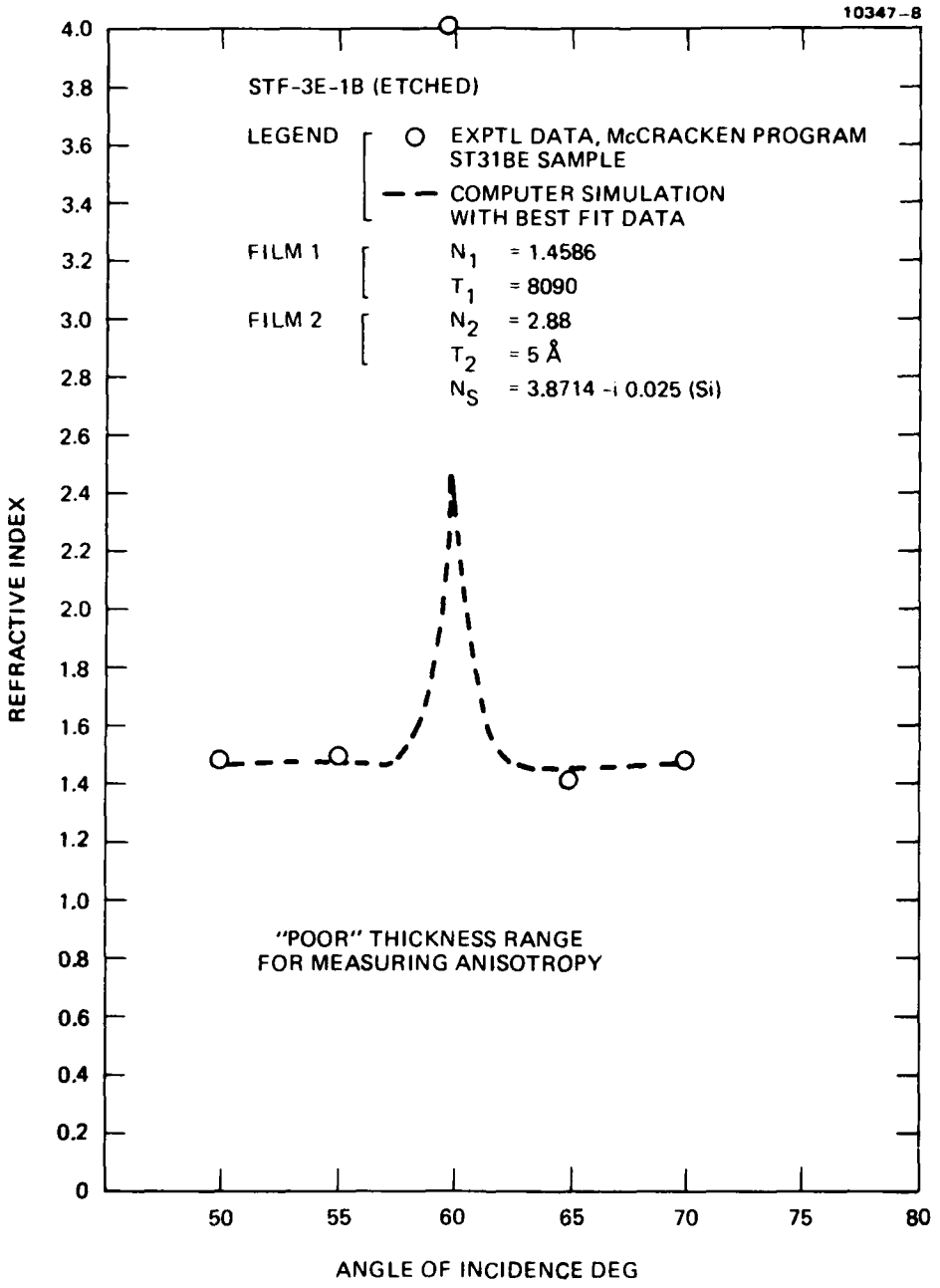

Figure 12. Refractive index versus angle unannealed film SiO_2 on Si "poor" thickness range for measuring anisotropy.

Table 6. Multiple Angle Ellipsometric Analysis of 6500Å and 9000Å Oxide Layers on Silicon

Sample Identification	Data Fitting Δ Error, Deg	ψ Error, Deg	Film #1 Thickness, (T_1) Å	Film #1 Index (N_1)	Film #1 Anisotropy ΔN_1	Film #2 Thickness, (T_2) Å	Film #2 Index (N_2)	Film #1 Stress (σ) Dynes/cm^2	Sample Condition Code Oxidation, Annealed
STF-15-E	0.09	0.09	9132	1.461	-0.00051	3	2.8	1.43×10^9	E-0
STF-15-C	0.11	0.11	6544	1.461	-0.00030	0.5	3.0	8.43×10^8	E-0
STF-15-C	0.14	0.14	6444	1.461	0	0.5	3.0	0	E-0
STF-15-C	0.30	0.16	6544	1.461	0	0	0	0	E-0

OXIDATION CODE

A	Wet, 1000°C Pulled Fast
B	Wet, 1100°C Pulled Slowly
C	Wet, 1100°C Pulled Fast
D	Dry, 1100°C Pulled Fast
E	Wet, 925°C Pulled Fast

ANNEALING CODE

1	925°C, 15 min
2	925°C, 30 min
3	925°C, 60 min
4	925°C, 120 min
5	1000°C, 30 min
6	1000°C, 60 min
0	No Anneal

and they can lead to measurement errors. A test for the existence of this effect will be to rotate the sample about an axis normal to and coincident with the measured spot. This rotation of the sample does not change the region of measurement.

The anisotropy value and the corresponding stress levels observed for these samples are in good agreement with the measurements made on the 11,800 Å films. The inner layer parameters seem to be in conflict here. It is possible that the film thickness regions that are optimum for stress measurements may not be optimum for measuring inner layer parameters.

5. The Limiting Film Thickness Experiment: 2500 Å and 2800 Å Film Thickness

The computer simulation convergence results presented in Figure 4 show that measurements made on oxide films that are thinner than 2500 Å should give no useful results. In fact the optimum thickness value to be used should be in the range 2700 Å ±25 Å. We prepared and measured samples with film thickness values ranging from 2468 Å to 2940 Å to evaluate empirically the feasibility of measuring anisotropy under this limiting sensitivity condition. The results of this study are presented in Table 7 for those oxide films with thicknesses near 2500 Å and in Table 8 for those oxide films with thicknesses near 2800 Å.

Samples STF-14-10, -14-10A, and -14-10B are different positions on the same wafer. The two samples with the lowest ψ convergence error show no anisotropy; the sample with the higher ψ convergence error also shows very little anisotropy. Since all of these convergence errors are small and the oxide film had been processed to yield maximum strain and anisotropy, we can conclude that this film thickness is a poor one for evaluating anisotropy. This is in very good agreement with Figure 4. The same conclusion applies to sample STF-14-2.

Samples STF-14-4A and -14-6A show excellent Δ and ψ convergence error levels, but one exhibits a small negative anisotropy and the other a small positive anisotropy. These films were both prepared in the same sample run and they were annealed for the same time period but at slightly different temperatures. Thus they should show smaller anisotropy than

Table 7. Multiple Angle Ellipsometric Analysis of 2500Å Thickness Silicon Oxide Layers on Silicon

Sample Identification	Data Fitting Δ Error, Deg	ψ Error, Deg	Film #1 Thickness, (T_1) Å	Film #1 Index (N_1)	Film #1 Anisotropy ΔN_1	Film #2 Thickness, (T_2) Å	Film #2 Index (N_2)	Film #1 Stress (σ) Dynes/cm^2	Sample Condition Code Oxidation, Annealed
STF-14-10	0.077	0.023	2521	1.4646	0	4	2.36	0	D-0
STF-14-10A	0.083	0.084	2520	1.4650	-0.000008	4	2.4	-2.247×10^7	D-0
STF-14-10B	0.084	0.025	2530	1.4603	0	4	2.37	0	D-0
STF-14-2	0.097	0.027	2468	1.4639	0	5	2.81	0	D-5
STF-14-4A	0.07	0.06	2510	1.463	-0.000014	5	2.43	-3.933×10^7	D-6
STF-14-6A	0.06	0.08	2526	1.4626	0.000013	4	2.33	3.652×10^7	D-3

OXIDATION CODE

A	Wet, 1000°C Pulled Fast
B	Wet, 1100°C Pulled Slowly
C	Wet, 1100°C Pulled Fast
D	Dry, 1100°C Pulled Fast

ANNEALING CODE

1	925°C, 15 min
2	925°C, 30 min
3	925°C, 60 min
4	925°C, 120 min
5	1000°C, 30 min
6	1000°C, 60 min
0	No Anneal

Table 8. Multiple Angle Ellipsometric Analysis of 2800Å Thick Silicon Oxide Layers on Silicon

Sample Identification	Data Fitting Δ Error, Deg	ψ Error, Deg	Film #1 Thickness, (T_1) Å	Film #1 Index (N_1)	Film #1 Anisotropy ΔN_1	Film #2 Thickness, (T_2) Å	Film #2 Index (N_2)	Film #1 Stress (σ) Dynes/cm^2	Sample Condition Code Oxidation, Annealed
STF-12-1	0.16	0.14	2940	1.4594	0	6	3	0	C-5
STF-12-1B	0.16	0.14	2937	1.4610	0	4	2.42	0	C-5
STF-12-2	0.029	0.029	2906	1.4595	-0.000059	4	2.22	-1.657×10^8	C-0
STF-12-2B	0.10	0.11	2897	1.4621	0	5.5	3.0	0	C-0
STF-12-3	0.13	0.13	2788	1.4586	0	6	3.1	0	A-5
STF-12-3B	0.15	0.18	2797	1.4590	0.003	3	1.8	8.427×10^8	A-5
STF-12-4	0.11	0.11	2775	1.4574	-0.0023	5.5	3.0	-6.461×10^8	A-0
STF-12-4B	0.13	0.11	2773	1.4581	0	5.5	3.0	0	A-0

OXIDATION CODE

A	Wet, 1000°C Pulled Fast
B	Wet, 1100°C Pulled Slowly
C	Wet, 1100°C Pulled Fast
D	Dry, 1100°C Pulled Fast

ANNEALING CODE

1	925°C, 15 min
2	925°C, 30 min
3	925°C, 60 min
4	925°C, 120 min
5	1000°C, 30 min
6	1000°C, 60 min
0	No Anneal

the ST31 samples but the anisotropies should be at least a factor of 30 larger (0.004) than they are in Table 4. Again we must conclude that this is a poor film thickness for evaluating anisotropy.

The results of measurements made on samples STF-12-1 and -12-2 are again questionable because this is a poor film thickness for measuring anisotropy. But from another point of view, they corroborate the theory because they show poor anisotropy resolution at a film thickness where it is expected to be bad. Samples STF-12-3 and -12-4 are 73 to 97 Å away from the optimum limiting film thickness of 2700 Å. These measurements, made at two different positions on each sample surface, yield conflicting results for two points on the same sample and different results from sample to sample. The large Δ and ψ convergence error levels shown by most of these samples will permit a wider range of anisotropy values to be fitted to the data. Thus one sample shows either 0 or a large positive anisotropy near 2700 Å, and another shows either 0 or a large negative anisotropy at a film thickness near 2700 Å. The method is again clearly not reliable at this film thickness, in agreement with theory.

6. The 1400 Å Device Type Oxide Film

Many silicon device structures are made with oxide thicknesses of about 1400 Å. The theoretical convergence error drive studies, summarized in Figure 4, show that anisotropy measurements made on films of this thickness should be poor but that the sensitivity for measuring inner layer parameters should be acceptable. The results are given in Table 9. The measurements on sample STF-11-5 showed large anisotropy and poor Δ, ψ convergence. The STF-11-5A data are a repeated measurement at another sample position which showed better Δ, ψ convergence and about half the anisotropy. This result shows that poor Δ, ψ convergence levels can lead to large errors in determining the anisotropy value. The positive sign on the anisotropy indicates that the measurement is wrong because it represents the oxide film in tension rather than compression. The results of measurements on samples STF-11-6 and

Table 9. Multiple Angle Ellipsometric Analysis of 1400Å Silicon Oxide Layers on Silicon

Sample Identification	Data Fitting Δ Error, Deg	ψ Error, Deg	Film #1 Thickness, (T_1) Å	Film #1 Index (N_1)	Film #1 Anisotropy ΔN_1	Film #2 Thickness, (T_2) Å	Film #2 Index (N_2)	Film #1 Stress (σ) Dynes/cm^2	Sample Condition Code Oxidation, Annealed
STF-11-5	0.18	0.15	1420	1.4610	+0.0012	4	2.44	3.3776×10^9	B-0
STF-11-5A	0.087	0.058	1431	1.4596	+0.00065	4	2.47	1.826×10^9	B-0
STF-11-6	0.098	0.055	1456	1.4590	+0.0011	4	2.40	3.090×10^9	B-2
STF-11-18	0.097	0.099	1568	1.4610	+0.0036	4.5	2.13	1.011×10^{10}	E-2

OXIDATION CODE

A	Wet, 1000°C Pulled Fast
B	Wet, 1100°C Pulled Slowly
C	Wet, 1100°C Pulled Fast
D	Dry, 1100°C Pulled Fast
E	Wet, 925°C Pulled Fast

ANNEALING CODE

1	925°C, 15 min
2	925°C, 30 min
3	925°C, 60 min
4	925°C, 120 min
5	1000°C, 30 min
6	1000°C, 60 min
0	No Anneal

-11-8 are also in error because of the positive anisotropy values. Again the theoretical prediction for this film thickness range is that the anisotropy should be difficult to observe. The measurement, on the other hand, shows anisotropy with low Δ, ψ convergence errors. Note, the anisotropy has the wrong sign. This result is an enigma. The faint possibility exists that the oxide has a different composition because it was grown at a lower temperature or was not strained as much as previous samples because of its lower growth temperature, and that the positive anisotropy relates to a lattice mismatch strain induced anisotropy rather than a thermal expansion coefficient mismatch effect.

7. Double Silicon Oxide Layers on Silicon

When a series of ordinary ellipsometric measurements were made on a 100 Å thick SiO_2 film on silicon as a function of the angle of incidence, a serious discrepancy in the measured refractive index of the oxide was observed.[5] These data are shown in Table 10. When these data were processed using the multiple angle ellipsometric method and allowing for two film layers on a silicon substrate, a new set of values was obtained for the oxide film parameters. These values are listed in Table 11. The oxide film index obtained by the multiple-angle method here is 1.49, whereas in the single angle results of Table 3 it ranges from 1.56 to 1.92. This value is still larger than a value of 1.45 measured for many other oxide samples. The value of the substrate refractive index is also slightly different from that usually observed for silicon (3.8714 - i0.025). It is possible that the thin oxide measured here has a slightly different refractive index than the thicker oxides usually measured for device work, but it is more likely that the SiO_2 layer was coated with a contaminant layer. If this is true, then the analysis of a three-layer system was performed with a two-layer model, yielding some inaccuracy. The most significant result here is the evaluation of the inner layer with a thickness of 6 Å and an index of 2.50. Finding a 6 Å layer under a 97 Å layer with an accuracy of 1 Å is very important for device modeling studies.

Table 10. Ellipsometric Evaluation of a Thin Oxide Layer on Silicon as a Function of the Angle of Incidence

Angle, deg			N_R	
70	150.766	11.42[illegible]	1.[illegible]	[illegible]
67.5	158.880	14.859	1.[illegible]	[illegible]
65	163.664	17.839	1.[illegible]	[illegible]
62.5	166.726	20.863	1.[illegible]	[illegible]
60	168.909	23.431	1.638	91.[illegible]
57.5	170.763	25.[illegible]	1.[illegible]	[illegible]
55	172.092	27.617	1.563	93.5
52.5	173.212	29.765	1.55[illegible]	93.[illegible]
50	174.087	31.470	1.644	90.[illegible]

Table 11. Multiple Angle Ellipsometric Evaluation of Silicon Oxides on a Silicon Substrate

Silicon oxide (SiO_2) layer thickness	97 Å
Silicon oxide layer index	1.49
Inner layer (SiO_x) thickness	6 Å
Inner layer (SiO_x) index	2.50
Substrate index, real part	3.858
Substrate index, imaginary part	-0.003

Thick Silicon Nitride Film

We have shown in previous sections that multiple-angle ellipsometry can be used to fit data taken on SiO_2 films on silicon substrates. We have also applied the method to the measurement of Si_3N_4 films on silicon with surprising results. Table 12 presents the ellipsometric data taken at various angular positions and processed with the conventional program. Notice, the measured refractive index and thickness do not change with angle of incidence. Our experience with SiO_2 on Si and its SiO_x inner layer would lead us to speculate that such a result indicates that no inner layer exists between the Si_3N_4 silicon substrate. However, these angle invariant results would also be obtained if an inner layer were present with a refractive index close to that of the Si_3N_4 film.

Table 13 shows the results of multiple-angle ellipsometric data fitting of the data in Table 12. Two film models were evaluated. The first included the Si_3N_4 film and the Si substrate; the second added an inner layer. The results were very similar in both cases. It is significant that the best fit (i.e., lowest convergence level) occurs for the case with no inner layer, and that the assumed presence of an inner layer does not alter the film thickness and index values obtained. A finite inner layer in the data reduction process alters the substrate index, but the inner layer and the substrate in this case are so close in index that the inner layer produces almost no measurable ellipsometric effect. This is in keeping with the results of ordinary ellipsometry, where slight changes in the value of the substrate index used in processing the data do not significantly alter the measured film thickness or index. Our conclusion, therefore, is that the existence of a SiO_x inner layer is possible but it must have a refractive index closer to that of Si_3N_4 (2.00) than to Si (4.8-j). In this case the index of 3.4 is not an unreasonable value for the inner layer, but it is not a proven value.

Table 12. Conventional Ellipsometric Measurements of the Refractive Index Thickness of Silicon Nitride Films on Silicon

Angle ϕ, deg	$\overline{\Delta}$	$\overline{\psi}$	$\overline{N_R}$	$\overline{T}$
70	9.1824	42.676	1.999	924.5
67.5	12.210	42.145	2.000	924.5
65	15.926	41.484	2.001	924.0
62.5	20.532	40.745	2.001	924.0
60	26.259	39.811	2.005	924.0
57.5	32.977	38.680	2.002	924.0
55	41.106	37.451	2.002	924.0
52.5	50.546	36.134	2.002	924.0
50	61.010	34.943	2.002	923.5

Table 13. Multiple Angle Ellipsometric Measurements for a Silicon Nitride Film on a Silicon Substrate

	Case 1	Case 2
Silicon nitride film index	2.000	2.000
Silicon nitride film thickness, Å	925.9	924.3
Inner layer film index	0	2.40
Inner layer film thickness, Å	0	1.9
Silicon substrate real index	3.8663	3.8663
Silicon substrate imaginary index	-0.0170	-0.0170
Multiple-angle convergence level	0.0839	0.9856
Comments	Model with Si_3N_4 film and substrate only	Model with Si_3N_4 film and inner layer

E. EXPERIMENTAL RESULTS — SILICON ON SAPPHIRE

The SOS samples were measured with a sample holder which had been extensively modified. The modifications consisted of replacing the sample holding vacuum chuck with a rotating stage, which also contained a vacuum chuck. This new feature made it possible to rotate the sample during the alignment process. This adjustment was vital in the case of SOS because the properties of the film (especially the film thickness) vary from point to point. Moreover, rotation of the sample is required for alignment of the optical axis of the sapphire substrate. If the optical axis of the substrate lies in the plane of incidence, then the conversion of P polarization to S polarization is minimized and vice versa. The presence of polarization mixing due to sample misalignment or misorientation gives rise to a lack of sensitivity in the nulling instrument and to significant errors in interpreting the data.

After the sample was mounted on the rotating stage, the polarizer was set to 0°, the compensator waveplate was removed, and the analyzer is set for 90°. The sample was then alternately rotated and tilted until the electronic detector showed a minimum. The compensator waveplate was then installed, and the data were obtained by the usual ellipsometric process of adjusting the polarizer and analyzer for the lowest null.

Because of the ambiguous nature of the orientation flat on one edge of each wafer, these samples were rotated to obtain four orthogonal wafer orientation positions where minimum polarization state mixing occurred; and Δ, Ψ versus ϕ data were taken at each of these angular positions. These data were processed in the standard ellipsometer data processing routine to obtain the refractive index and thickness at each angular position. Data are plotted in Figure 13 for sample 10 rotated through positions 1, 2, 3, and 4. These data sets are labeled 10-1, 10-2, 10-3 and 10-4 for simplicity. It is evident that the SOS 10-1 data is the best behaved as a function of angle. This characteristic has also been observed for SiO_2 films on silicon in thickness ranges where the sensitivity for measuring anisotropy was high.

The data from sample 10-1 were analyzed in the three-layer anisotropic program, and the results are given in Table 14. We find here a native oxide or contamination layer 7 Å thick with an index of 1.4 on top of a 4656 Å

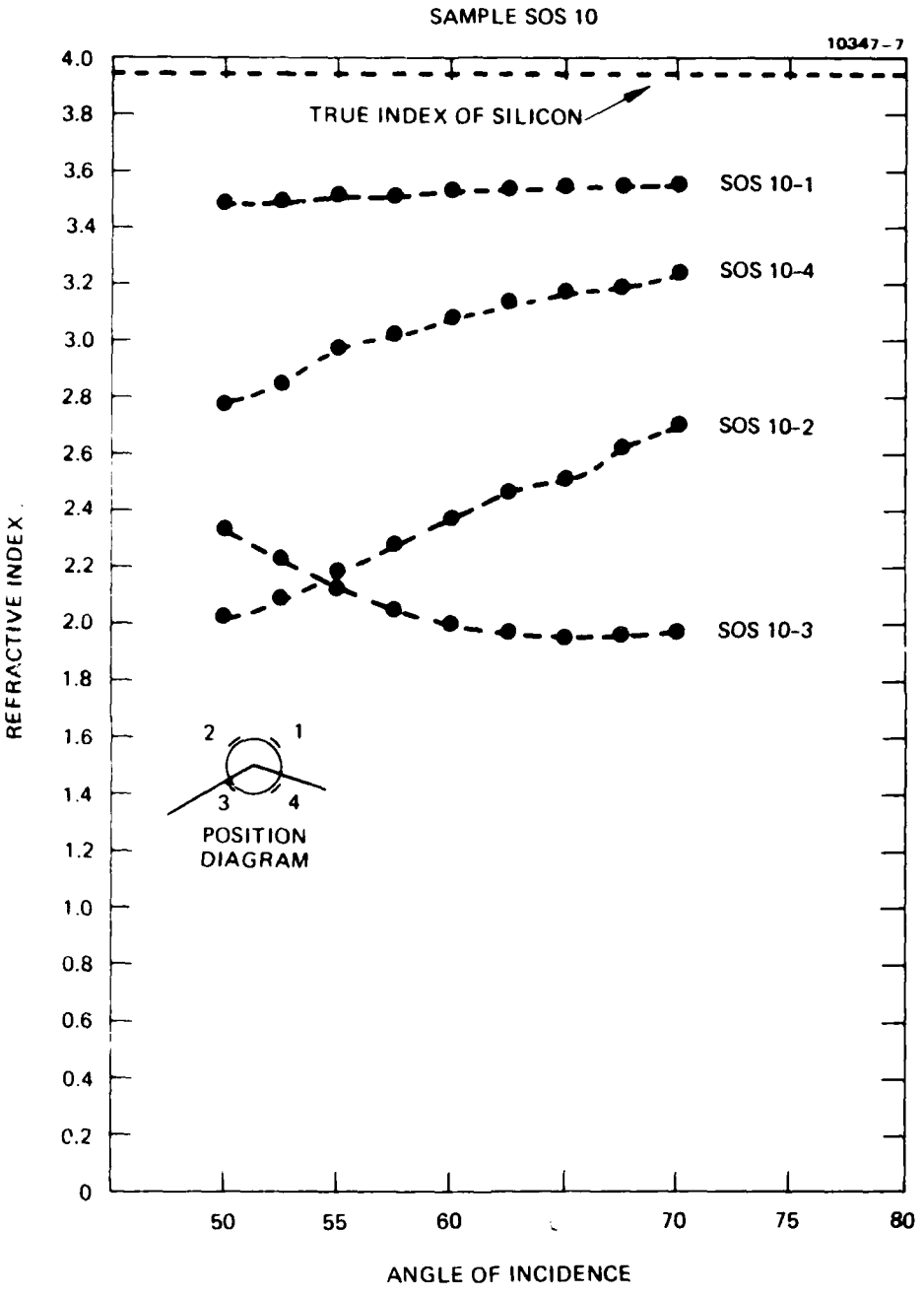

Figure 13. Measured silicon index versus angle ϕ for four principle plane orientations

Table 14. Multiple Angle Ellipsometric Analysis of 4600Å Silicon Layer on Sapphire

Sample Identification	Data Fitting Δ Error Deg	ψ Error Deg	Film #1 Thickness, (T_1) Å	Film #1 Index N_1	Film #2 Anisotropy ΔN_A	Film #1 Anisotropy ΔN_B	Film #2 Thickness, (T_2) Å	Film #2 Index N_2	Film #2 Stress (σ_A) Dynes/cm^2	Film #2 Stress (σ_B) Dynes/cm^2
SOS-10-1	0.068	0.071	7	1.400	0.073	0.017	4656	3.997	11.1×10^9	2.58×10^9
SOS-12-3	0.700	0.500	26	1.450	0	0.20	4813	3.902	0	3.04×10^9
SOS-13-4	0.080	0.080	53	1.42	0.018	0.0031	4546	3.911	2.73×10^9	0.47×10^9
SOS II-C	0.410	0.120	28	1.5	0.005	0	4030	3.891	0.76×10^9	

OXIDATION CODE

A	Wet, 1000°C Pulled Fast
B	Wet, 1100°C Pulled Slowly
C	Wet, 1100°C Pulled Fast
D	Dry, 1100°C Pulled Fast

ANNEALING CODE

1	925°C, 15 min
2	925°C, 30 min
3	925°C, 60 min
4	925°C, 120 min
5	1000°C, 30 min
6	1000°C, 60 min
0	No Anneal

silicon layer. This silicon layer has an index of 3.997 and has an anisotropy of 0.017 in the plane of the film and of 0.073 perpendicular to the plane of the film. (A schematic of the anisotropy geometry is given in Figure 14.) This result corresponds to a stress four times larger across the film than normal to the film. This large orthogonal stress in the silicon film is caused by local Si-Al_2O_3 interface shifts which relieve stresses and introduce shear strain components in the plane of the film. Recently, Abrhams et al.[17] reported enormous shear stresses, of the order of 2×10^{10} dyn/cm^2, near threefold interface regions of silicon, sapphire, and vacuum. These shear stresses exceed compressive stresses by an order of magnitude. Since the elasto-optic effect is usually smaller for shear strain than for longitudinal strain, the effect of shear strain on the anisotropy induced in the silicon film is smaller than that due to the longitudinal strain. Thus the observation of a second anisotropy component with a magnitude 1/4 that of the thermal expansion stress induced anisotropy in our experiment is not unreasonable, and it corroborates the existence of the shear strains in silicon.

The magnitude of the major anisotropy component σ_A, and the minor component σ_B were translated into film stress values using estimates of the elasto-optic constants of silicon at 6328 Å. Silicon materials are basically opaque at this wavelength, and the stress optic constants have not been reported. The compressive and shear stress values are thus estimated to be 9×10^9 and 2×10^9 dyn/cm^2. The compressive stress value is in good agreement with the work of Kamins,[18] who reports values of 6 to 9×10^9 dyn/cm^2. The shear stress value is, of course, incorrect since the shear elasto-optic tensor effect is much smaller than the compressive elasto-optic effect.

The ellipsometric results for samples SOS-12-2 and -13-4 are also given in Table 14. The results for sample SOS-13-4 are easily compared with sample SOS-10-1 analyzed earlier because the convergence levels are almost the same. The anisotropies are quite different in these two samples, and in fact the relative sizes of the anisotropies for in the plane and out of the plane are interchanged. This is not unexpected for SOS samples because the shear stress is reported to vary by an order of magnitude from point to point across the sample.[17] Sample SOS-12-2 requires a large in-plane anisotropy, but the level of convergence is poor (0.70, 0.50). It is possible that a large component of

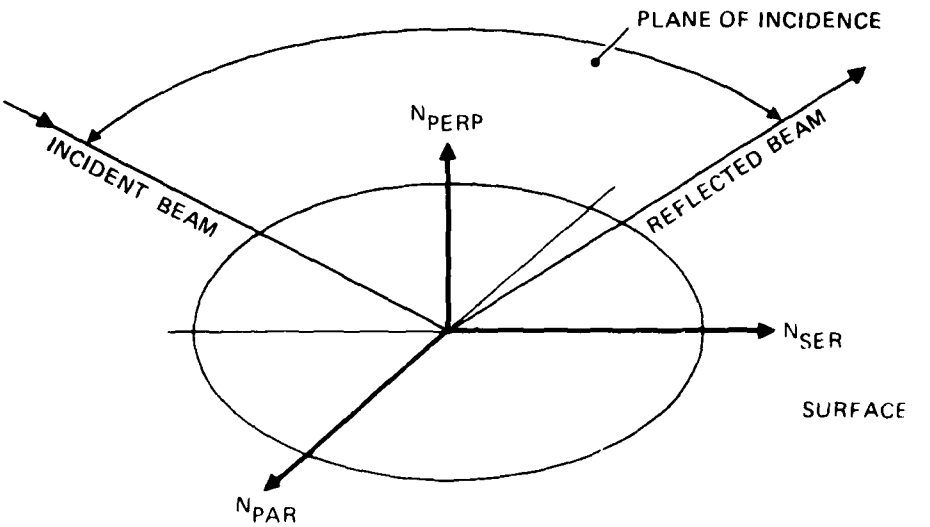

$$\Delta N_1 \quad N_{PAR} - N_{PERP}$$

$$\Delta N_2 \quad N_{PAR} - N_{SER}$$

$$\text{NORMAL CONDITION} \begin{cases} N_{PAR}\ N_{SER} & M_o \\ N_{PERP} & N_e \end{cases}$$

$$N_{PERP} = N_o - N_1$$

$$N_{SER} = N_o - \Delta N_2$$

$$N_{PAR} = N_o$$

Figure 14. Refractive index anisotropy geometry.

strain in the silicon film lies at an angle to the plane of incidence of the ellipsometer. This would give rise to strong polarization state mixing and a good degree of convergence.

1. Early SOS Results

Figure 15 presents the results of ordinary ellipsometric measurements made on wafer SOS II. In these measurements, the position of the wafer was changed three times, and the wafer was rotated for a minimum polarization state mixing condition. The results for sample positions a, b, and c are quite different. Of the three data sets, the sample position and orientation labeled SOS showed the least variation with angle, and SOS IIC was the only data set that could be crudely fitted with the programming available at that time. Although the refractive index variation with angle for SOS IIC is about a factor of two larger than that shown earlier for SOS 101, it is still much smaller than that obtained for orientations IIa and IIb. It is this behavior of the measured refractive index with angle of incidence and sample orientation angle that provides a clue as to the usability of the experimental SOS data. After enough of SOS samples have been measured, it will be possible to identify the appropriate orientation of the sample for best data convergence. The confusion here is that the flat edge on the sapphire wafer is oriented at $\pm 45^\circ$ to the projection of the C axis of the sapphire. The C axis is oriented relative to the plane at a specific angle for best lattice matching. Thus there are four possible sample orientations and only two can be correct. When these early data were taken, this was not well understood and the optimum orientation was not measured.

Another problem with the early SOS work was that the index of silicon was kept fixed during the data processing because it was assumed that the anisotropy was small. This prevented obtaining the optimum convergence of the data.

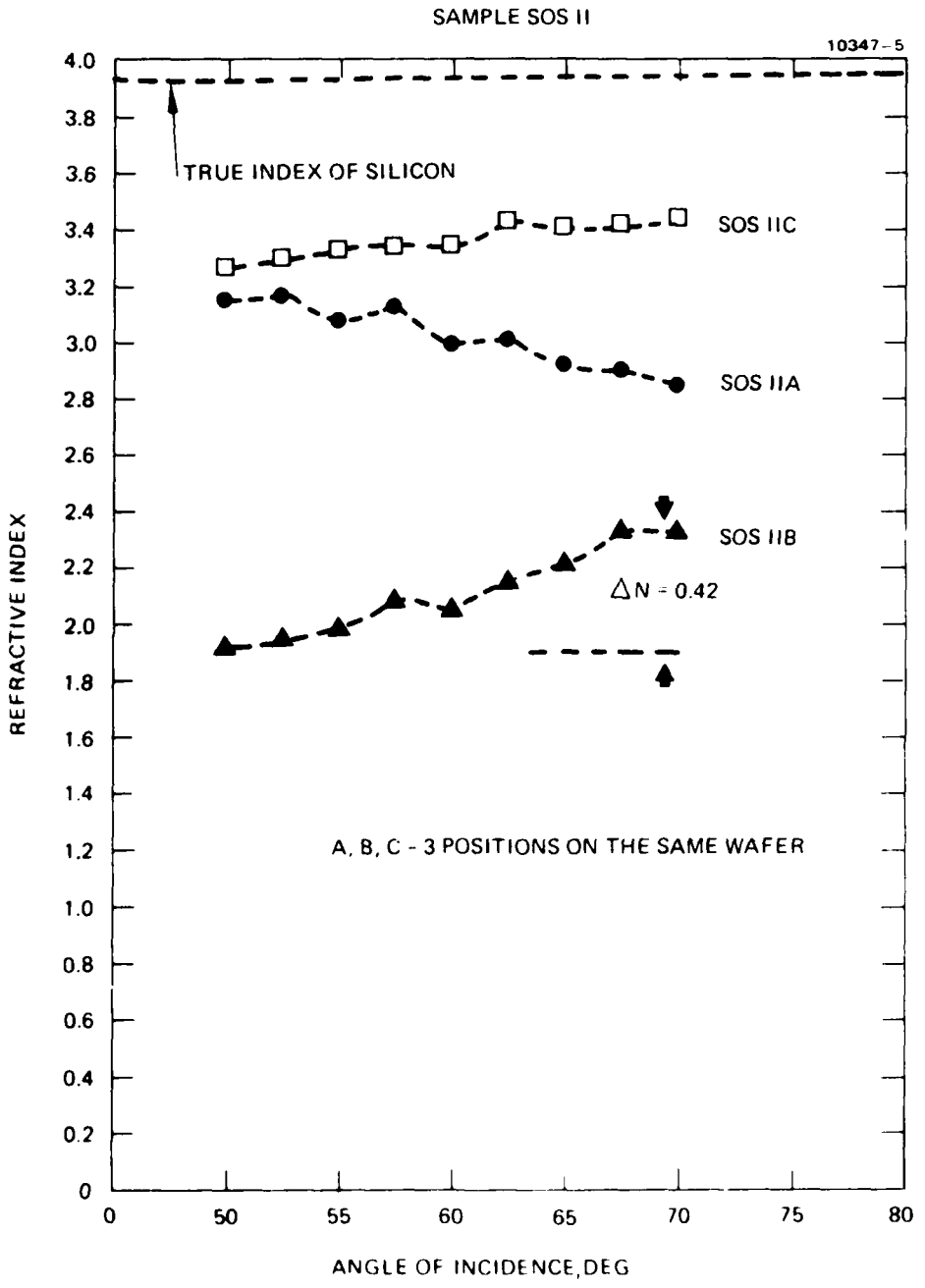

Figure 15. Measured silicon index versus angle ; for three sample orientations.

2. Conclusions on Anisotropy in SOS

Allowing the refractive index to vary and using two anisotropies improved the convergence, as the latest SOS data show. The combined results for the SOS measurements lead to the following conclusions:

- Large optical anisotropy exists in epitaxial silicon films grown on sapphire substrates, and these anisotropies are measurable using ellipsometry.

- The anisotropy can have components along each of three coordinate axes; if this coordinate system is not aligned with the plane of incidence of the ellipsometer, polarization state mixing will occur and our anisotropic model will not be able to interpret the data.

- These optical anisotropy components are generated by compressive thermal stresses in the sapphire films and by local shifting of the films, which allows stress relaxation and shear strain components.

- These shear strain components have large magnitudes but their elasto-optic effect is not as large as that due to the compressive strains generated by thermal stress. Hence the change in refractive index generated by shear stresses in the film are not to be simply compared with the changes in refractive index due to thermal stress.

- This ellipsometric method developed for evaluating stress in SOS films has led to an evaluation of the anisotropy in these films and can be further exploited as a tool for evaluating the quality of these films.

SECTION 3

CONCLUSIONS AND DISCUSSION

A. ELLIPSOMETRIC STRESS MEASUREMENT

The goal of this investigation was to develop an ellipsometric method for measuring stress in single-layered thin oxide films on silicon. We achieved this goal and in the process also developed a method for evaluating double-layered optically transparent films. This was needed because the thermal oxide grown on silicon is composed of a thin SiO_x transition layer and a thicker SiO_2 layer. The multiple-angle ellipsometric measurement system developed here is capable of evaluating the thickness, index, and anisotropy of the oxide layer as well as the index and thickness of the transition layer. The method is limited to specific film thickness regions for good accuracy in measuring the anisotropy in the oxide, but it works almost everywhere in evaluating the other parameters.

This method has also been modified in order to evaluate three-layer films and has been applied in a preliminary way to the measurement of stress in epitaxial silicon films on sapphire. The SOS system consists of a set of three layers on a sapphire substrate. The silicon layer lies closest to the sapphire followed by layers of SiO_x and SiO_2. The results of the measurements on SOS indicate that the data cannot be fitted without using anisotropy values on the order of 3%. This is 30 times larger than for the oxide on silicon. Another surprising result of this study is that the anisotropy values vary drastically from point to point on the surface of the sapphire, which we believe to be due to local variations in film thickness and to random detachment of the silicon from the sapphire, causing shear stresses to be generated in the silicon films.

B. STRESS IN THERMAL OXIDES

Ellipsometric stress measurements were made on all oxidized samples listed in Table 1. The resulting data are summarized in Table 15 and described more fully in Section 2.D.

Table 15. Inner Layer and Stress in Oxide Samples

Wafer	Anisotropy	Stress	Inner Layer		Oxide	
		dyne/cm^2	Thickness, Å	Index	Thickness, Å	Index
STF- 3- 1A	-0.00071	-2.0×10^9	5	2.16	11,820	1.461
- 1B	-0.00088	-2.5×10^9	5	2.[illegible]	11,850	1.460
- 2A	-0.00051	-1.4×10^9	5	2.[illegible]	11,680	1.462
- 2B	-0.00090	-2.5×10^9	5	2.[illegible]	11,720	1.460
STF-3E- 1A	-0.000031	-8.7×10^7	[illegible]	[illegible]	8,090	1.458
- 1B	0	0		[illegible]	8,090	1.459
- 2A	0	0		[illegible]	8,[illegible]	1.458
- 2B	0	0		[illegible]	8,[illegible]	1.459
STF-11- 5	0.0012	$+3.4 \times 10^9$	4	2.[illegible]	1,420	1.461
- 5A	0.00065	$+1.8 \times 10^9$	4	2.[illegible]	1,430	1.460
- 6	0.0011	$+3.1 \times 10^9$	4	2.40	1,460	1.459
-18	0.0036	$+1.0 \times 10^{10}$	4.5	2.13	1,570	1.461
STF-12- 1	0	0	6	3	2,940	1.459
- 1B	0	0	4	2.42	2,940	1.461
- 2	-0.000059	-1.7×10^8	4	2.22	2,910	1.460
- 2B	0	0	5.5	3.0	2,900	1.462
- 3	0	0	6	3.1	2,790	1.459
- 3B	0.003	$+8.4 \times 10^8$	3	1.8	2,800	1.459
- 4	-0.0023	-6.5×10^8	5.5	3.0	2,780	1.457
- 4B	0	0	5.5	3.0	2,770	1.458
STF-14- 2	0	0	5	2.81	2,470	1.464
- 4A	-0.000014	-3.9×10^7	5	2.43	2,510	1.464
- 6A	-0.000013	-3.7×10^7	4	2.33	2,530	1.463
-10	0	0	4	2.36	2,520	1.465
-10A	-0.000008	-2.2×10^7	4	2.4	2,520	1.465
-10B	0	0	4	2.37	2,530	1.460
STF-15-C	-0.00030	-8.4×10^8	0.5	3.0	6,540	1.461
-E	-0.00051	-1.4×10^9	3	2.8	9,130	1.461

The sensitivity of the stress measurement technique is limited to certain ranges of oxide thickness (see Section 2.B). Inspection of Table 15 indicates that only the wafers in lots STF-3 and -15 fall in the high-sensitivity ranges. Therefore, only those wafers are considered to indicate oxide stress values accurately.

Figure 16 is a plot of measured oxide stress versus oxide thickness for as-grown thermal oxides in lots STF-3 and -15. All of these wafers were grown at 1100°C in a wet O_2 ambient and rapidly quenched after oxide growth. The data indicates that stress increases monotonically with oxide thickness over the range from 6,500 to 12,000 Å. This is reasonable since the thinner oxides are more deformable and can flex to relieve the inherent thermal strain. The data square in Figure 16 shows the excellent agreement between the ellipsometric stress measurement and the value measured in Reference 1 for a (100) oxide grown in wet O_2. The slightly higher value given in Reference 1 may be due to the higher growth temperature (1200°C versus 1100°C for this work).

The effect of a 925°C N_2 anneal on the interfacial stress is shown in Figure 17. The indicated stress reduction may be due to a re-equilibration of the Si/SiO_2 system at a lower temperature than the growth temperature (1100°C) and a concomitant reduction in the cooling range from equilibrium to room temperature. The re-equilibration mechanism may be a viscous flow of the oxide, although studies have indicated that the viscous SiO_2 state is restricted to temperatures above 965°C. Alternatively, the stress relaxation may be associated with damage annealing at the Si/SiO_2 interface.

C. CAPACITANCE-VOLTAGE MEASUREMENTS

Lots STF-11 and STF-14 were subjected to C-V measurements to determine a correlation between surface state concentration at the Si/SiO_2 interface and growth conditions. Table 16 summarizes the growth/anneal conditions for the wafers in each of these lots and the measured Q_{ss}/q. Lot STF-11 consists of a wet oxidation of n-type Si, while STF-14 is a dry oxidation of p-type Si.

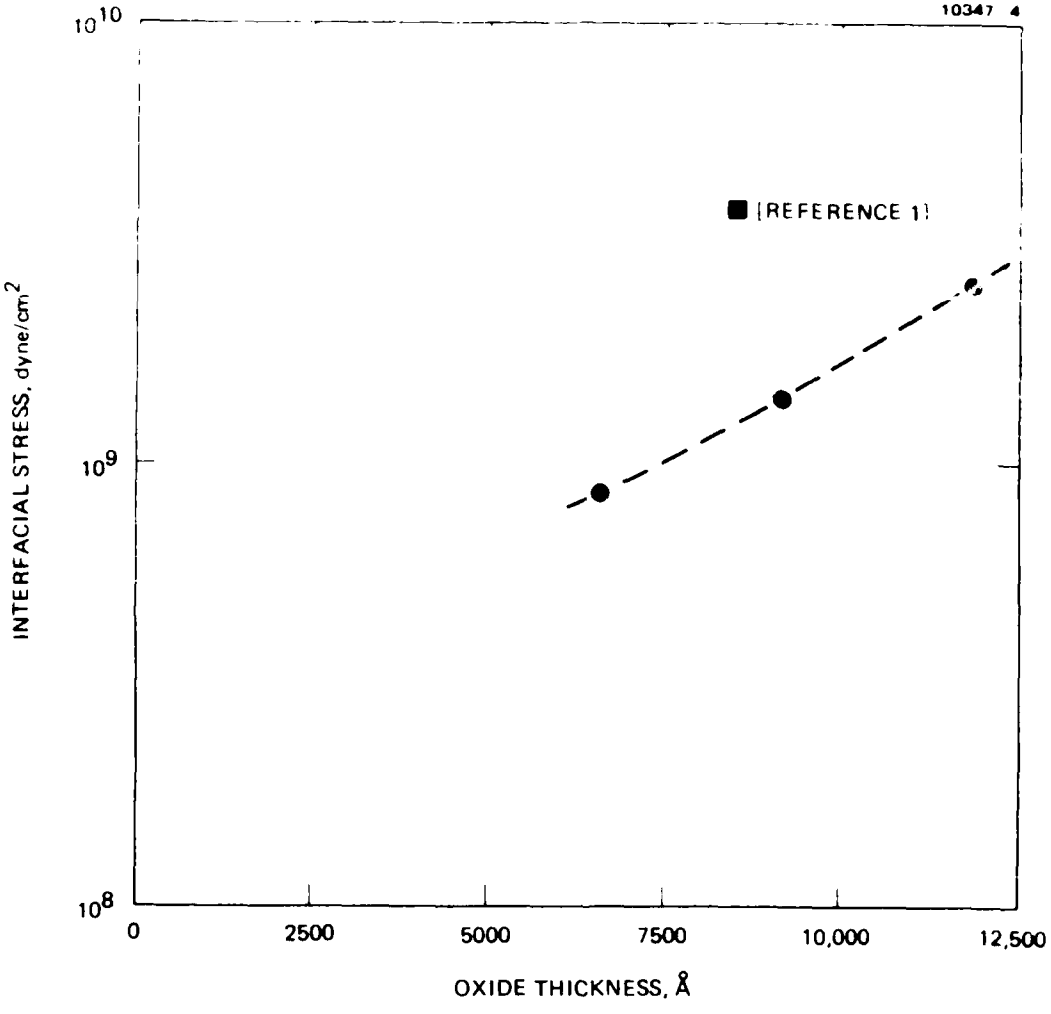

Figure 16. Interfacial stress in Si/SiO_2 system versus oxide thickness, as grown at 1100°C.

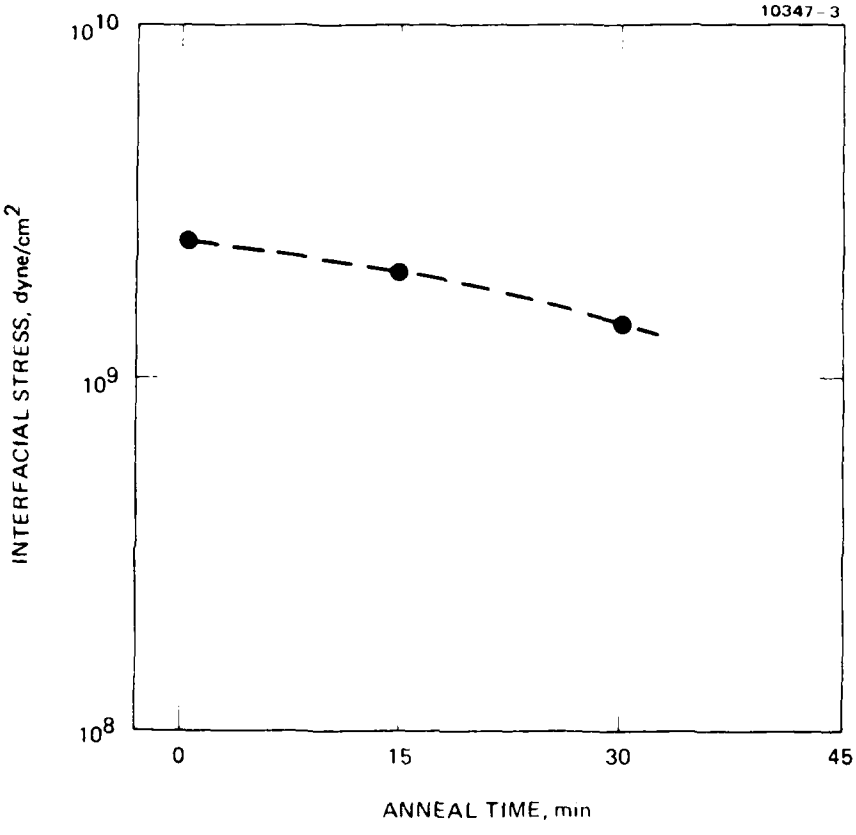

Figure 17. Interfacial stress in Si/SiO_2 system versus anneal time at 925°C.

Table 16. Oxide Growth and Anneal Conditions, and Measured Surface State Concentrations for Lots STF-11 and STF-14

Wafer	Type	Oxidation Conditions			Anneal Conditions		Q_{ss}/q, $cm^{-2} \times 10^{10}$
		Temp, °C	Wet/Dry	Quench	Temp, °C	Time	
STF-11- 1	n	1100	W	Y	—	—	2.9
STF-11- 2	n	1100	W	Y	925	30	6.6
STF-11- 5	n	1100	W	N	—	—	0.8
STF-11- 6	n	1100	W	N	925	30	1.9
STF-11- 9	n	1000	W	Y	—	—	-0.8
STF-11-10	n	1000	W	Y	925	30	0.2
STF-11-13	n	1000	W	N	—	—	5.8
STF-11-14	n	1000	W	N	925	30	0.1
STF-11-17	n	925	W	Y	—	—	2.0
STF-11-18	n	925	W	Y	925	30	1.4
STF-11-21	n	925	W	N	—	—	6.7
STF-11-22	n	925	W	N	925	30	6.3
STF-14- 1	p	1100	D	Y	1000	30	-0.9
STF-14- 3	p	1100	D	Y	1000	60	-1.1
STF-14- 5	p	1100	D	Y	925	60	0
STF-14- 7	p	1100	D	Y	925	120	-0.4
STF-14- 9	p	1100	D	Y	—	—	1.2

Surface-state concentrations in lot STF-11 range from -0.82×10^{10} to 0.7×10^{10} cm^{-2} with no apparent correlation with growth conditions. Figure 18 shows attempts to correlate the measured Q_{ss}/q with growth temperature, quench rate, and anneal temperature. No correlation is observable with any of these variables. The range of Q_{ss}/q found in lot STF-11 is apparently due to irregularities in cleaning and handling or to process non-uniformities during sample preparation. No conclusions can be reached relating surface-state concentration to oxide growth conditions from lot STF-11.

C-V measurements were also made on a p-type lot, STF-14. All wafers in this lot were oxidized in dry O_2 and quickly quenched after oxidation (Table 16). The lot was then split and annealed under varying conditions. Figure 19 shows plots of Q_{ss}/q versus both anneal time and temperature. These graphics indicate a strong decrease in Q_{ss}/q with increasing anneal time and temperature.

The oxide thicknesses targeted for lots STF-11 and STF-14 were subsequently found to be within a range in which stress measurements could not be made reliably (see Section 2.B). Therefore, no attempt was made to correlate the observed C-V data with interfacial stress. Without this additional information, the source of the interface state density variations in lots STF-11 and STF-14 cannot be uniquely identified.

D. STRESS IN SOS FILMS

Ellipsometric stress measurements were made on various SOS wafers graded by Union Carbide according to film quality; the data are summarized in Table 17. The quality grades seem to correlate most closely with compressive stress values in the three samples drawn in the table. The highest-quality sample ("no haze") contains the most stress, with the poorest-quality wafer ("medium haze") showing no measurable compressive stress. This would indicate that slippage at the Si/Al_2O_3 interface is the stress reduction mechanism in SOS, resulting in a lowered value of stress, but highly damaged Si. These data suggest an SOS quality assurance technique that might be useful: measuring stress in SOS films using the non-destructive ellipsometric technique to ascertain quickly the quality of the grown epitaxial film.

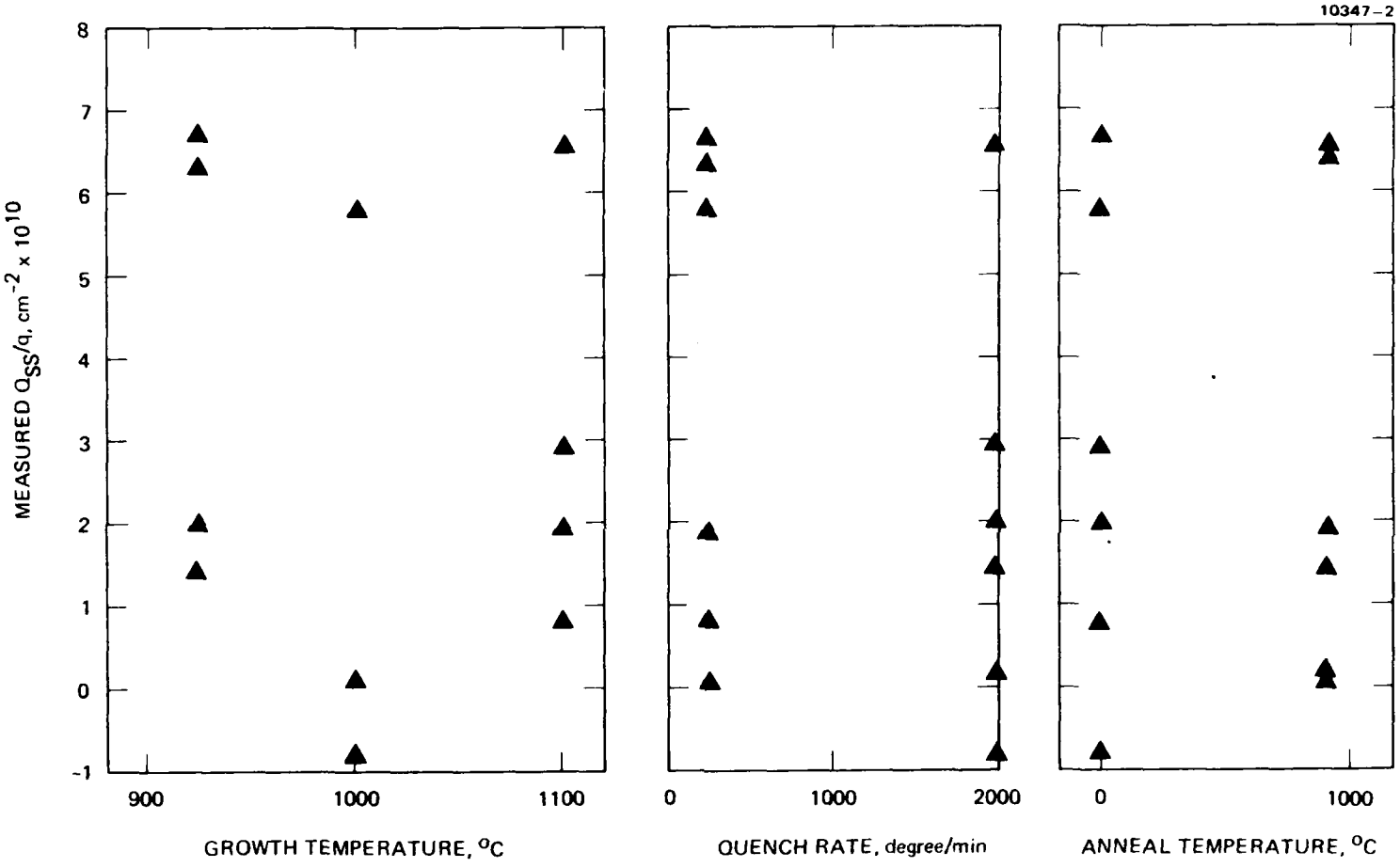

Figure 18. Correlation of measured surface state density with oxide growth and anneal conditions for lot STF-11.

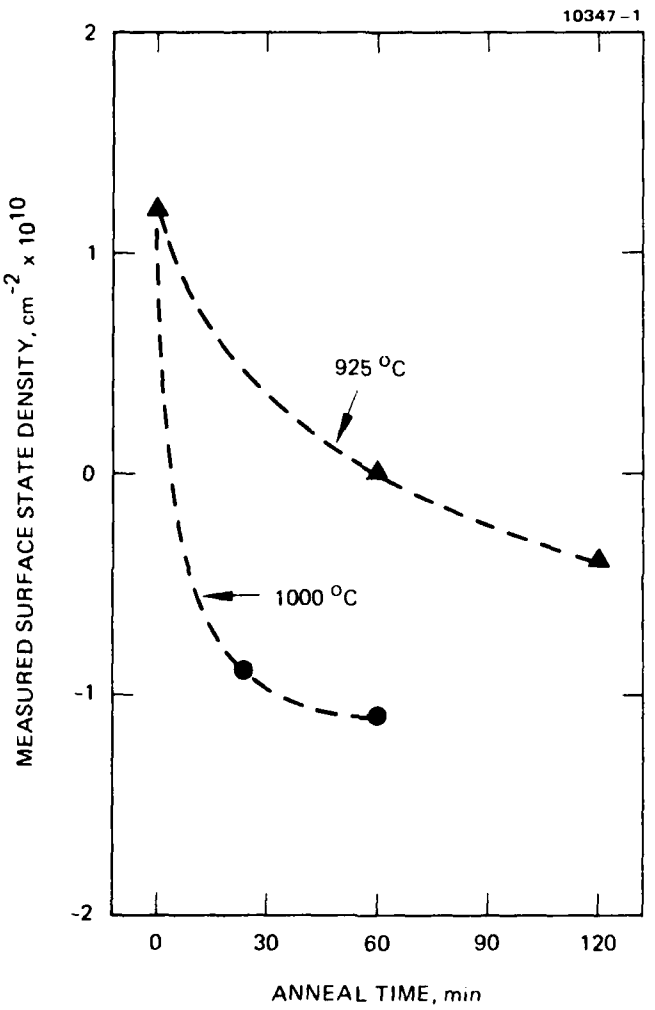

Figure 19. Correlation of measured surface state density with oxide anneal conditions for lot STF-14.

Table 17. Stress and Quality Grade in SOS Samples

Wafer	Si Index	Si Thickness, Å	Anisotropy		Compressive Stress, dyne/cm^2	Shear Stress, dyne/cm^2	Grade
			Δn_1	Δn_1			
SOS-10-1	4.00	4660	0.073	0.017	1.1×10^{10}	2.6×10^{9}	No haze
SOS-12-2	3.90	4810	0	0.020	0	3.0×10^{9}	Medium haze
SOS-13-4	3.91	4550	0.018	0.0031	2.7×10^{9}	4.7×10^{8}	Very light haze

As discussed in Section 2.E, a high degree of convergence in the SOS data analysis program requires that the local anisotropy in the film align with the coordinate system determined by the wafer surface and the plane of light incidence. No data are presented from wafer SOS-11 because no position on this wafer could be found to yield reliably convergent data. In addition, the poor convergence of the SOS-12 data is believed to be due to this nonalignment problem.

APPENDIX A

EXPERIMENTAL METHOD

[illegible] silicon wafers were mounted in a Rudolph nulling-type [illegible] and aligned and measured according to the manufacturers instructions. Care was taken to ensure that the same "spot" on the film was measured at each angle of incidence to avoid variations in film thickness and stress from point to point on the surface of the film. The experimental data were taken using the four-quadrant method[15] for highest accuracy and to provide a self-consistancy check at each angle of incidence. The data were then processed to obtain Δ and ψ and stored in the computer. The multiple-angle anisotropic data processing program was then applied to the data set. In this procedure, the "operator" selects parameter search ranges for film thickness, refractive index, and anisotropy and for substrate refractive index. The machine then calculates and displays the values of the parameters that fit the experimental data best and the degree of fit in terms of the least-squares error in Δ and ψ. The operator can iterate two parameters at a time to find the optimum fit and he can make a permanent record of the experimental data and the parameters that best fit the data. If the data does not converge well, a second subroutine is available; this subroutine uses the best fit index, thickness, and anisotropy data to generate a set of Δ, ψ values to compare with the experimental Δ, ψ data set. The differences are automatically printed, and any gross discrepancies are easily observed. These erroneous data points can be eliminated to form a new, truncated data set with better convergence properties. Whenever this method of data diagnosis has not worked, we have assumed that the number of layers used in the data processing model was incorrect.

APPENDIX B

THE EFFECT OF STRAIN-INDUCED ANISOTROPY IN THIN FILMS ON THE REFLECTION OF POLARIZED LIGHT

A. INTRODUCTION

The existence of optically anisotropic thin film structures and their measurement by ellipsometric techniques have been reported by Den Engleston.[19] The films investigated consisted of an array of monomolecular layers of well-oriented molecules[20] which exhibit an anisotropy unrelated to the properties of the substrate. We have reported the observation of strain-induced anisotropy in optical films.[14] This effect is attributed to lattice mismatch and thermal expansion coefficient differences between the film and the substrate which give rise to strain in the film. The nature of the stress and the attendant strain generated in thin films by this mechanism has been widely investigated,[14,21-25] and stresses on the order of 4×10^9 dyn/cm^2 have been observed in both compression and tension. A calculation of the change in film refractive index using this stress level and the bulk elasto-optic constants of common optical film materials where available shows that the change in refractive index should be less than 0.5%.

An electromagnetic analysis of reflection from a uniaxial anisotropic film with the optic axis of the film orthogonal to the plane of the film has been given by Den Engleston.[19] We have expanded and applied his model to a calculation of two specific anisotropy cases: perpendicular anisotropy (in which the optic axis is perpendicular to the surface of the film and parallel to the plane of incidence) and planar anisotropy (in which the optic axis lies in the plane of the film and is perpendicular to the plane of incidence).

We have not evaluated the third case, in which the optic axis lies in the plane of the film and is parallel to the plane of incidence, because it is expected to produce results similar to the case where the optic axis is normal to the plane of the film.

These three orientations of the optic axes for a uniaxial material are of special theoretical interest in that they preserve the s and p polarization states of the incident radiation: all other orientations mix in the polarization states. This mixing leads to extreme complication both mathematically and experimentally.

B. STRESS-INDUCED OPTICAL ANISOTROPY IN THIN FILMS

If a thin isotropic film of one solid material is deposited on a substrate of another solid material at an elevated temperature, and if the materials have different thermal expansion coefficients, then strain will exist at the boundary between these materials after they have cooled to an ambient temperature.[27-29] This would be true even if both materials had matching lattice spacing, but the presence of lattice mismatch effects can either add to or subtract from the thermally induced strain.[29] It is the presence of strain in the film (and substrate) which gives rise to optical anisotropy in the film (and substrate) via the elasto-optic effect. The theory of the elasto-optic effect is described in general by a sixth rank tensor[28] which relates the change in refractive index in the medium to a strain induced in the medium. For materials that are optically isotropic, the optical symmetry conditions reduce the complexity of this matrix. The independent variables in these matrices, the elastic stresses or strains, are themselves fourth-rank tensors which are simplified by the conditions of elastic isotropy.[30] An evaluation of the elastic tensor in terms of the elastic constants of the film is needed befor the elasto-optic tensor can be employed.

C. ANALYSIS

Analysis of an anisotropic film is in general very difficult due to the admixture of r and s polarized fields by the anisotropy of the film. However, a more tractable problem occurs if the film exhibits uniaxial properties and if the unique axis is either perpendicular to the surface of the film (perpendicular case) or parallel to the plane of the film and orthogonal to the plane of incidence (planar case). Using the coordinate system of Figure B-1 for these two cases, the index tensor can be expressed as:

$$\bar{\bar{N}} = \begin{pmatrix} N_{or} & 0 & 0 \\ 0 & N_{or} & 0 \\ 0 & 0 & N_{ex} \end{pmatrix} \quad \text{for the perpendicular case}$$

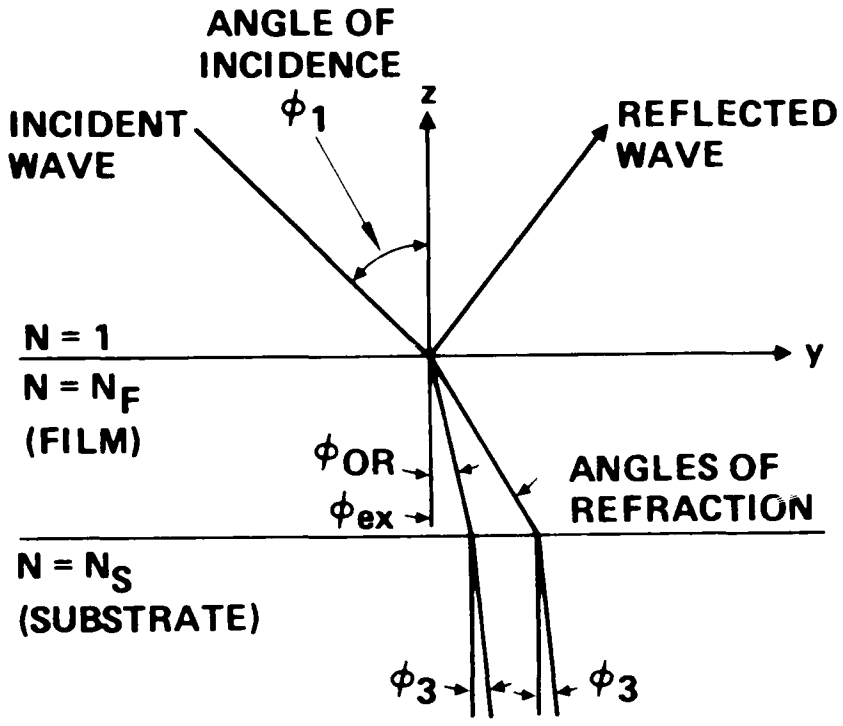

Figure B-1. Theoretical model of anisotropic film.

$$\bar{\bar{N}} = \begin{pmatrix} N_{ex} & 0 & 0 \\ 0 & N_{or} & 0 \\ 0 & 0 & N_{ex} \end{pmatrix} \quad \text{for the planar case.}$$

We will assume that the films and substrates are transparent in all cases.

1. Planar Anisotropy

To calculate the reflection coefficients for the r and s polarizations of the film substrate system requires calculating the Fresnel coefficients of the interfaces and the phase factor associated with traversal of the film for each polarization. At the first interface (air-film), the reflection coefficients are of the form

$$r_{\perp}^{(1)} = \frac{\cos \phi_1 - N_{ex} \cos \phi_{ex}}{\cos \phi_1 + N_{ex} \cos \phi_{ex}} \tag{B.1}$$

$$r_{\parallel}^{(1)} = \frac{\cos \phi_{or} - N_{or} \cos \phi_1}{\cos \phi_{or} + N_{or} \cos \phi_1} \tag{B.2}$$

at the film-substrate interface. Here and below, the symbols are as defined in Table B-1.

$$r_{\perp}^{(2)} = \frac{N_{ex} \cos \phi_{ex} - N_s \cos \phi_3}{N_{ex} \cos \phi_{ex} + N_s \cos \phi_3} \tag{B.3}$$

$$r_{\parallel}^{(2)} = \frac{N_{or} \cos \phi_3 - N_s \cos \phi_{or}}{N_{or} \cos \phi_3 + N_s \cos \phi_{or}} \tag{B.4}$$

Table B-1. Symbols

F_t	*film thickness*
λ	wavelength in free air
N_s	index of substrate
N_{or}	ordinary index of refraction of the film
N_{ex}	extraordinary index of refraction of the film
ϕ_1	angle of incidence
ϕ_{or}	angle of refraction in the film of the ordinary polarization
ϕ_{ex}	angle of refraction in the film of the extraordinary polarization
ϕ_3	angle of refraction in the substrate
$R_\perp$	the reflection coefficient of film substrate for s polarization
$R_\parallel$	the reflection coefficient of the film substrate for p polarization
β_{or}	phase factor for the ordinary wave
β_{ex}	phase factor for the extraordinary wave

The phase factors associated with the two polarizations are

$$\beta_\perp = \frac{2\pi F_t}{\lambda}\left(N_{ex}^2 - \sin^2\phi_1\right)^{1/2} \qquad (B.5)$$

$$\beta_\parallel = \frac{2\pi F_t}{\lambda} N_{or}\cos\phi_{or} \qquad (B.6)$$

The total reflection coefficients can then be calculated from

$$R_\perp = \frac{r_\perp^{(1)} + r_\perp^{(2)} e^{-2j\beta}}{1 + r_\perp^{(1)} r_\perp^{(2)} e^{-2j\beta}} \qquad (B.7)$$

and

$$R_{\parallel} = \frac{r_{\parallel}^{(1)} + r_{\parallel}^{(2)} e^{-2i\beta_{\parallel}}}{1 + r_{\parallel}^{(1)} r_{\parallel}^{(2)} e^{-2i\beta_{\parallel}}} \qquad (B.8)$$

All angles other than ϕ_1 can be eliminated from $R_{\perp}$ and $R_{\parallel}$ by using Snell's law:

$$\sin \phi_1 = N_{or} \sin \phi_{or} = N_{ex} \sin \phi_{ex} = N_s \sin \phi_3 \quad . \qquad (B.9)$$

The ratio of $R_{\parallel}$ to $R_{\perp}$ can be used to find the usual ellipsometric variables Δ and ψ from:

$$\frac{R_{\parallel}}{R_{\perp}} = \tan \psi \, e^{i\Delta} \qquad (B.10)$$

If a stress orthogonal to the plane of incidence is applied to the substrate film combination, anisotropy can be induced in the film index. The form of this anisotropy corresponds to our model of the planar case.

In principle, an unstressed film could be measured, a clamp (or equivalent) used to stress the film in a fixture, and then the film remeasured. The problem with this approach is that thermal effects in the fixture and additional experimental uncertainties limit the accuracy of the results.

2. Perpendicular Anisotropy

Isotropic films deposited on isotropic substrates will, in general, be anisotropic due to differential thermal expansion. Films are frequently deposited at elevated substrate temperatures and then cooled to room temperature. The differential thermal expansion between the film and substrate produces an isotropic stress in the plane of the film and therefore, because of the elasto-optic effect, produces optical anisotropy of the perpendicular form. In this case, the s-polarized wave always "sees" a constant index N_{or} as a function of angle of incidence. The p polarization component, however,

sees a varying index as a function of angle of incidence due to the anisotropy of the film. Again, just as in the planar case, to calculate the reflection coefficient of the film-substrate system only requires calculating the Fresnel coefficients at the interfaces and the phase factors for traversal of the film.

The Fresnel coefficients of the film air interface are

$$r_{\perp}^{(1)} = \frac{\cos \phi_1 - N_{or} \cos \phi_{or}}{\cos \phi_1 N_{or} + \cos \phi_{or}} \tag{B.11}$$

$$r_{\parallel}^{(1)} = \frac{\cos \phi_1 N_{or} N_{ex} - \left(N_{ex}^2 - \sin \phi_1\right)^{1/2}}{\cos \phi_1 N_{or} N_{ex} + \left(N_{ex}^2 - \sin^2 \phi_1\right)^{1/2}} \quad . \tag{B.12}$$

The Fresnel coefficients of the film substrate interface are

$$r_{\perp}^{(2)} = \frac{N_{or} \cos \phi_o - N_s \cos \phi_3}{N_{or} \cos \phi_o + N_s \cos \phi_3} \tag{B.13}$$

$$r_{\parallel}^{(2)} = \frac{N_s \left(N_{ex}^2 - \sin^2 \phi_1\right)^{1/2} - N_{or} N_{ex} \cos \phi_3}{N_s \left(N_{ex}^2 - \sin^2 \phi_1\right)^{1/2} + N_{or} N_{ex} \cos \phi_3} \quad , \tag{B.14}$$

and the phase factors for traversal of the film are

$$\beta_{\perp} = \frac{2\pi F_t}{\lambda} \left(N_{or}^2 - \sin^2 \phi_1\right)^{1/2} \tag{B.15}$$

$$\beta_{\parallel} = \frac{2\pi F_t}{\lambda} \frac{N_{or}}{N_{ex}} \left(N_{ex}^2 - \sin^2 \phi_1\right)^{1/2} \quad . \tag{B.16}$$

$R_\perp$ and $R_\parallel$ can be calculated as before:

$$R_\perp = \frac{r_\perp^{(1)} + r_\perp^{(2)} e^{i2\beta_\perp}}{1 + r_\perp^{(1)} r_\perp^{(2)} e^{i2\beta_\perp}} \tag{B.17}$$

$$R_\parallel = \frac{r_\parallel^{(1)} + r_\parallel^{(2)} e^{i2\beta_\parallel}}{1 + r_\parallel^{(1)} r_\parallel^{(2)} e^{i2\beta_\parallel}} \tag{B.18}$$

Inserting the expressions for the phase factors and the single surface Fresnel coefficients into Eqs. B.17, B.18, and B.10, $R_\perp$ and $R_\parallel$ can be used to calculate the parameters Δ and ψ. As before, all angular variables (ϕ_{or}, ϕ_{ex}, and ϕ_3) can be eliminated by using a modified Snell's law.

In our analysis, we neglected those elasto-optic tensor terms that describe the change in refractive index that occurs when a shear stress is applied to the crystal. These shear stresses will be present in the thin film[31] because the thermal expansion (contraction) stress is applied at the film substrate interface, and the opposite film surface is a stress-relief or stress-free surface. Under these conditions, a stress gradient is generated normal to the film, with concomitant shear stresses. In the absence of specific stress gradient data and elasto-optic data, a specific calculation of this effect is not feasible.

The equations derived here have also been applied to the case of three anisotropic films on an anisotropic substrate. The only tractable solutions were found for the case where the optic axis of the substrate is aligned in the plane of incidence. These equations are too lengthy to reproduce in this report.

APPENDIX C

PHOTOELASTICITY

A. THE STRESS-OPTIC EFFECT

The stress-optic effect was used in this study to convert refractive index anisotropy data into oxide film stress data. The theory of this effect applied to thermal expansion coefficient mismatch stress generated in thin films was presented in Ref. 14 and is summarized in Section C.II. The equations governing the change in refractive index due to stress are given by

$$\Delta N_1 = \frac{1}{2}\left(N_o\right)^3 \left(2q_{12}\right) \sigma \qquad (C.1)$$

$$\Delta N_2 = \frac{1}{2}\left(N_o\right)^3 \left(q_{11} + q_{12}\right) \sigma \qquad (C.2)$$

$$\Delta N_3 = \frac{1}{2}\left(N_o\right)^3 \left(q_{11} + q_{12}\right) \sigma \quad , \qquad (C.3)$$

where N_o is the refractive index of the film, and the q_{ij} are the stress optic tensors. The total anisotropy is defined in our programs by the equation

$$\Delta N = \Delta N_2 - \Delta N_1 = \Delta N_3 - \Delta N_1 = -\frac{1}{2}\left(N_o\right)^3 \left\{ q_{12} - q_{11} \right\} \sigma \quad . \qquad (C.4)$$

For SiO_2 films, the stress-optic factor is given by

$$\frac{\Delta N}{\sigma} = -\frac{\left(N_o\right)^3}{2} \left\{ q_{12} - q_{11} \right\} \quad . \qquad (C.5)$$

From the work of Primak and Post[32] and Waxler, Horowitz, and Feldman[33] the values of q_{11} and q_{12} are equal to 0.43×10^{-13} cm^2/dyn and 2.70×10^{-13} cm^2/dyn. The stress-optic factor is evaluated from Eq. C.4 using

these values of q_{11} and q_{12} and a value of 1.46 for the refractive index of the oxide:

$$\frac{\Delta N}{\sigma} = -3.55 \times 10^{-13} \text{ cm}^2/\text{dyn} \quad . \tag{C.6}$$

The stress constant is calculated from Eq. C.6:

$$\sigma = (-2.8 \times 10^{+12} \text{ dyn/cm}^2)\ \Delta N \quad . \tag{C.7}$$

The results measured for samples STF-3-1 and -2 yielded anisotropies over the range -0.00051 to -0.00090 and stress values over the range 1.43×10^9 dyn/cm^2 to 2.53×10^9 dyn/cm^2. The positive sign on the stress values indicate that they are compressive; this is in agreement with the linear thermal expansion for quartz and silicon. The silicon shrinks much more than the SiO_2 on cooling from 1100°C to 20°C and puts the SiO_2 film in compression.

In the case of silicon on sapphire, the stress-optic coefficients are not known at 6328 Å because the material is not transparent at this wavelength. Using Eq. C.5 and changing the refractive index from 1.46 (SiO_2) to 3.8714 (Si), we can estimate the stress-optic constant to be 1.511×10^{11} dyn/cm^2. The anisotropies measured for SOS samples were of the order of 0.07 yielding, stress levels of the order of 10^{10} dyn/cm^2 for Si or Al_2O_3.

B. THE ELASTO-OPTIC EFFECT

The change ΔN_i in the refractive index measured along a principal coordinate direction i produced by strains ε_j is given by

$$\begin{aligned}
\Delta N_1 &= -\frac{1}{2} (N_o)^3 (P_{11}\varepsilon_1 + P_{12}\varepsilon_2 + P_{12}\varepsilon_3) \\
\Delta N_2 &= -\frac{1}{2} (N_o)^3 (P_{12}\varepsilon_1 + P_{11}\varepsilon_2 + P_{12}\varepsilon_3) \\
\Delta N_3 &= -\frac{1}{2} (N_o)^3 (P_{12}\varepsilon_1 + P_{12}\varepsilon_2 + P_{11}\varepsilon_3) \quad ,
\end{aligned} \tag{C.8}$$

where P_{ij} is the elasto-optic tensor. In this analysis, the effect of shear strains is assumed to be negligible. A similar set of equations can be written for the relationship between the stress σ_1 and the strain ε_j induced in an elastic medium in terms of the compliance tensor S_{ij}:

$$\begin{aligned} \varepsilon_1 &= S_{11}\sigma_1 + S_{12}\sigma_2 + S_{12}\sigma_3 \\ \varepsilon_2 &= S_{12}\sigma_1 + S_{11}\sigma_2 + S_{12}\sigma_3 \\ \varepsilon_3 &= S_{12}\sigma_1 + S_{12}\sigma_2 + S_{11}\sigma_3 \quad . \end{aligned} \tag{C.9}$$

Eqs. C.8 and C.9 are valid for either an isotropic (solid such as fused quartz) or a cubic lattice (such as diamond or silicon). In the case of strain induced by thermal expansion (contraction) in a thin film, the stress normal to the surface of the film must be zero (i.e., $\sigma_1 = 0$) and the other stresses must be equal (i.e., $\sigma_2 = \sigma_3$). This reduces the strain equations to the form

$$\begin{aligned} \varepsilon_1 &= 2\, S_{12}\, \sigma_2 \\ \varepsilon_2 &= \varepsilon_3 = (S_{11} + S_{12})\, \sigma_2 \end{aligned} \tag{C.10}$$

and yields the relationship between the strain

$$\varepsilon_1 = \left[\frac{(2\, S_{12})}{(S_{11} + S_{12})}\right] \varepsilon_2 \tag{C.11}$$

normal to the plane of the film ε_1 and the strain parallel to the plane of the film ε_2. The strain in the film (and in the adjacent substrate) is calculated from the relationship.

$$\varepsilon_2 = \frac{\Delta \ell}{\ell} = (\alpha_s - \alpha_f)\, \Delta t \quad , \tag{C.12}$$

where α_f is the thermal expansion coefficient of the thin film, α_s is the thermal expansion coefficient of the substrate, and Δt is the temperature drop of the structure after fabrication. (An additional strain ε_2 can also occur due to lattice mismatch.) The symmetry arguments which led to Eq. (C.10) also simplify Eq. C.8 to the form

$$\Delta N_1 = -\frac{1}{2}\left(N_o\right)^3\left(P_{11}\varepsilon_1 + 2P_{12}\varepsilon_2\right)$$

$$\Delta N_2 = \Delta N_3 = -\frac{1}{2}\left(N_o\right)^3\left(P_{12}\varepsilon_1 + \left(P_{11} + P_{12}\right)\varepsilon_2\right) \quad . \qquad (C.13)$$

Using Eq. C.12 to evaluate ε_2, Eq. C.11 to evaluate ε_1, and Eq. C.13 to evaluate the refractive index changes ΔN_1 and ΔN_2, we can determine the anisotropy in the refractive index of a thin film generated by a difference in the thermal expansion coefficients of the film and substrate materials. Using the linear thermal expansion factor for silicon and SiO_2 over the thermal cooling range 1100°C to 20°C, the strain ε_2 in Eq. C.12 has the value -2.45×10^{-3} and the ratio of $\varepsilon_1/\varepsilon_2$ in Eq. C.11 has the value -0.375. Solving for the birefringence $\Delta N_2 - \Delta N_1$ of Eq. C.13, we obtain $\Delta N = \Delta N_2 - \Delta N_1 = -0.00036$. This estimate of the thermal expansion induced anisotropy in the oxide film lies slightly below the range of the anisotropy values measured for the oxide film on silicon. The additional anisotropy observed in these films may be due to lattice mismatch strain effects as well as to thermal expansion strain effects. The latter effects can be partially annealed out, but the former are permanent.

If the stress-optic constant $C = 3.56 \times 10^{-13}\ (dyn/cm^2)^{-1}$ is multiplied by the stress value $T = 2 \times 10^9\ dyn/cm^2$ observed in SiO_2 films by other methods,[32,33] the birefringence has a value of $N_o - N_e = -0.00070$, which falls near the top of the range of anisotropy values measured here. The fact that the total anisotropy predicted this way is larger than that predicted by thermal expansion theory supports the thesis that lattice mismatch effects increase the strain and the anisotropy.

APPENDIX D

RETROSPECTION: EARLY ANISOTROPY PREDICTIONS

In our earliest calculations of the effects of strain-induced anisotropy in oxide films on silicon, we used a simple model of an anisotropic oxide film on a silicon substrate. We calculated the ellipsometric parameters Δ and ψ for each oxide film thickness, and we processed the data in the National Bureau of Standards McCracken program to obtain a simulation of the measurement process. The results for two anisotropies are given in Figures D-1, D-2, D-3, and D-4. These curves predicted large deviations from the "true" refractive index at specific film thicknesses and specific angles of incidence.

When experimental measurements were performed on appropriate oxide samples, the data and the theory were widely divergent. A search of the scientific literature gave the results of Cordes and Taft[12] which evaluated the ellipsometric effect of an inner layer between the oxide layer and the silicon substrate. This layer produced deviations in the measured refractive index that were larger than those predicted for anisotropy alone. This result forced development of a new approach to the analysis of oxide films on silicon. The results of this effort are the multiple-angle ellipsometric techniques discussed earlier. The summary of the sensitivity of this method for evaluating anisotropy is given in Figure D-4.

Our early theoretical model for stress-induced anisotropy in films predicted that the changes in Δ and ψ due to stress would be most easily observable at multiples of the resonant film thickness given by the formula:

$$\Delta T = \frac{\lambda}{2}\left(N^2 - \sin^2 \phi\right)^{-1/2} ,$$

where λ is the optical wavelength, N is the refractive index of the film, and ϕ is the angle of incidence of the light. In the case of an SiO_2 film measured at an angle of incidence of 70°, ΔT has a value of 2832 Å. We see that ΔT corresponds to the first discontinuity in Figures D-1 and D-2. At this early period in the program, we mainly assumed that the "best" anisotropic effects would be observed at thicknesses that were integer or half-integer multiples of 2832 Å. We have plotted these thickness values as vertical lines on Figure D-4. It is interesting that some of these film thicknesses correspond

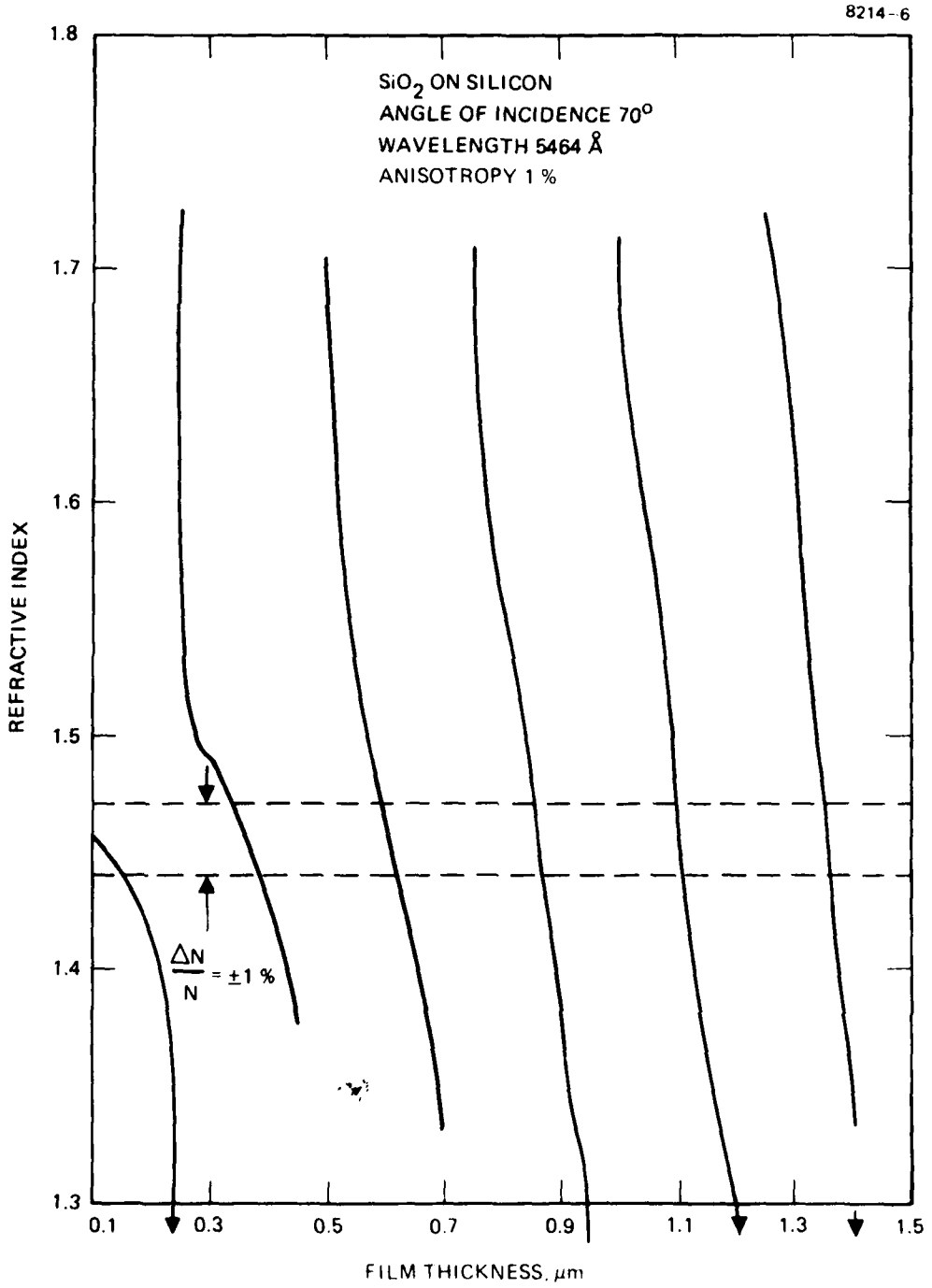

Figure D-1. Computer simulation of refractive index measured versus film thickness.

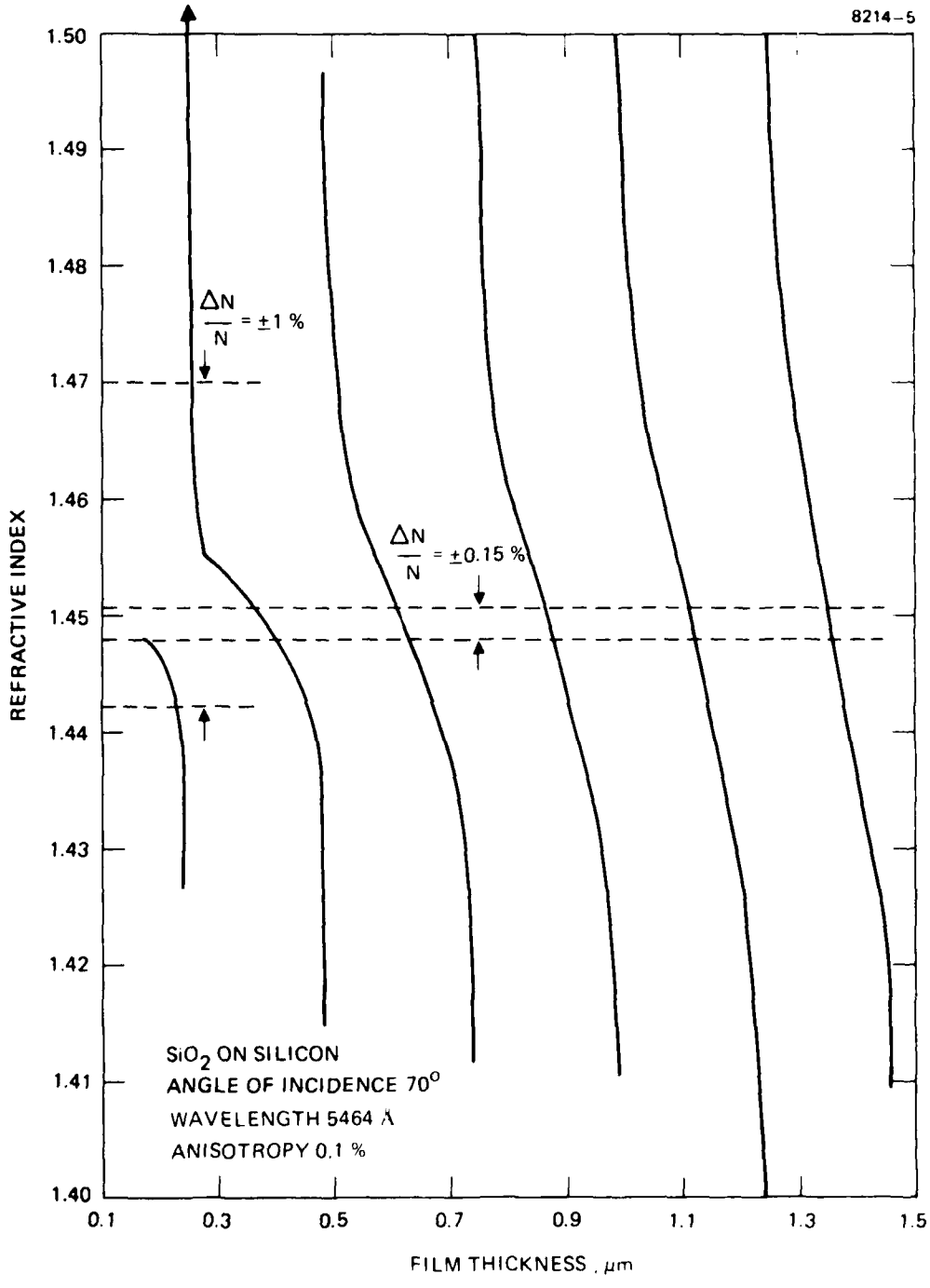

Figure D-2. Computer simulation of refractive index measured versus film thickness.

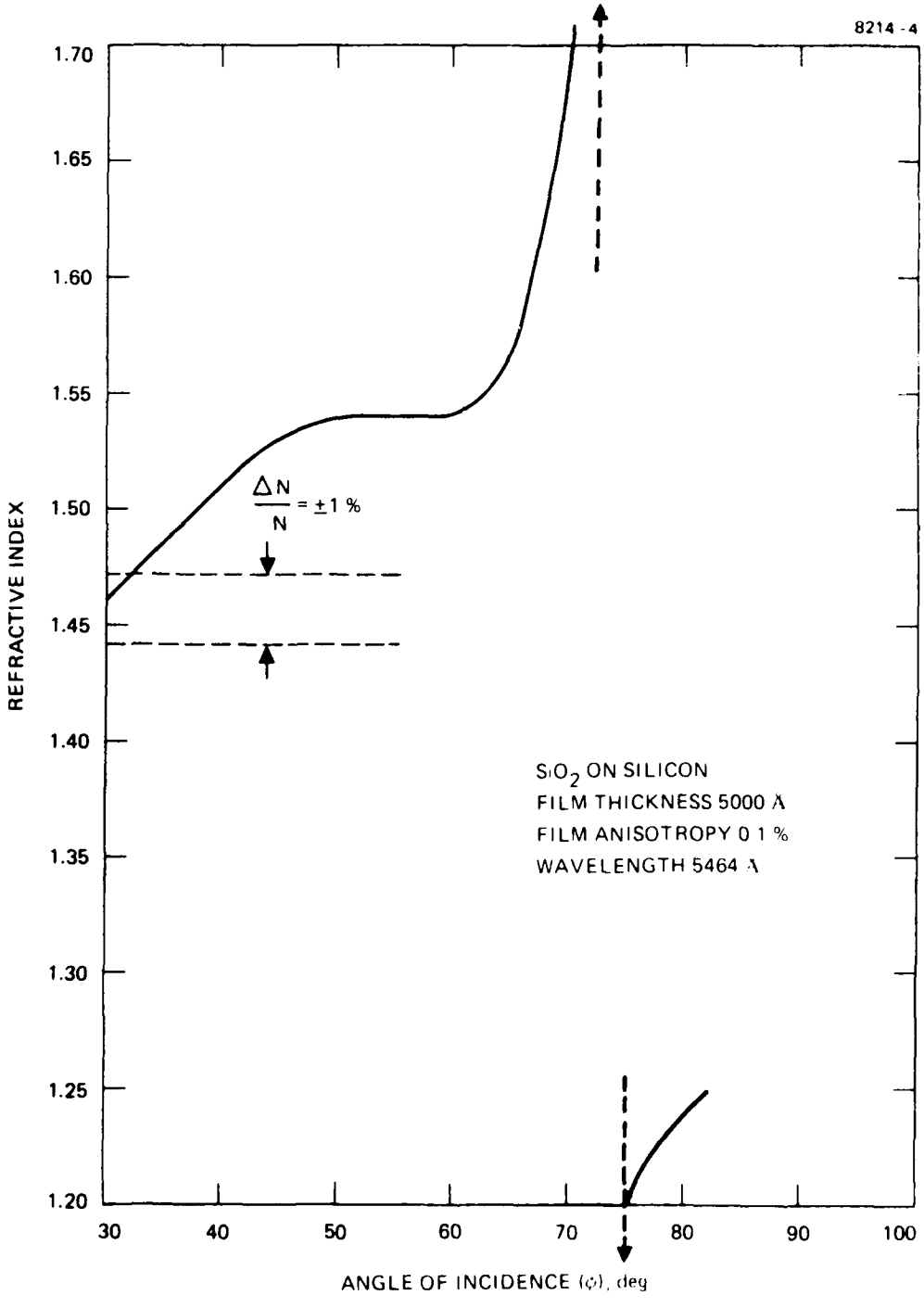

Figure D-3. Computer simulation of refractive index measured versus angle of incidence.

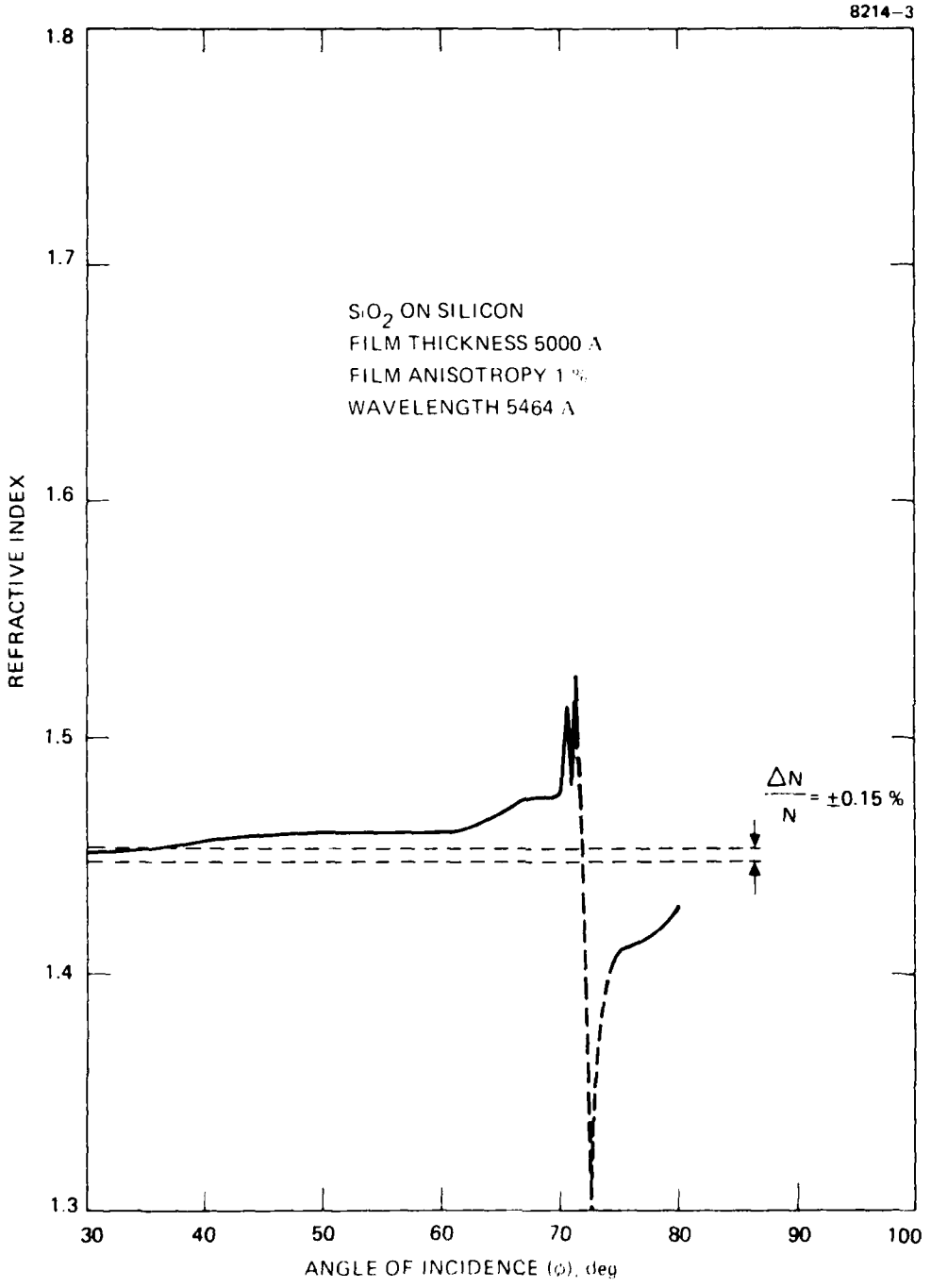

Figure D-4. Computer simulation of refractive index measured versus angle of incidence.

to "good" places to measure anisotropy and others to bad places. Thus the simple ΔT rule of thumb is not adequate for predicting the optimum film thickness for measuring anisotropy, but it was correct in about half of the cases. The growth of the sensitivity to anisotropy with increasing film thickness in Figure D-4 is not unexpected because the increased optical path length in thicker films gives rise to larger anisotropic phase shifts. The width of the maximum is probably due to the shifting together of adjacent peaks which would have existed in the absence of the inner layer effects.

REFERENCES

1. M.V. Whelan, A.H. Goemans, and L.M.C. Goossens, "Residual Stresses at an Oxide-Silicon Interface," Appl. Phys. Lett. 10, 262 (1967).

2. R.J. Jaccodine and W.A. Schlegel, "Measurement of Strains at Si-SiO_2 Interface," J. Appl. Phys. 37, 2429 (1966).

3. D.J. Dumin, "Deformation of and Stress in Epitaxial Silicon Films on Single-Crystal Sapphire," J. Appl. Phys. 36, 2700 (1965).

4. C.Y. Ang and H.M. Manasevit, "Residual Stress in Epitaxial Silicon Film on Sapphire," Sol.-St. Electronics 8, 994 (1965).

5. C.H. Lane, "Stress at the Si-SiO_2 Interface and Its Relationship to Interface States," IEEE Trans. on Electron Devices ED-15, 998 (1968).

6. A.J. Hughes and A.C. Thorsen, "Anisotropy in Electrical Properties of {001} Si/{0$\bar{1}$12}Al_2O_3," J. Appl. Phys. 44, 2304 (1973).

7. K. Bulthuis, "The Effect of Local Pressure on Silicon p-n Junctions," Phillips Res. Repts. 20, 415 (1965).

8. E.P. EerNisse and G.F. Derbenwick, "Viscous Shear Flow Model for MOS Device Radiation Sensitivity," IEEE Trans. on Nuclear Science NS-23, 1534 (1976).

9. I.J. Hodgkinson and A.R. Walker, "Stress Relief Induced in Silicon Oxide Films by Ultraviolet Radiation," Thin Sol. Films 17, 185 (1973).

10. J.H. Serebrinsky, "Stress Concentration in Silicon-Insulator Interfaces," Sol.-St. Electronics 13, 1435 (1970).

11. M.E. Pedinoff, D.C. Mayer, O.M. Stafsudd, and G. Dunn. "Multi Angle Ellipsometric Studies of Strained SiO_2 on Si", Electrochemical Society Meeting, Hollywood, Florida, 5-10 October 1980.

12. E. Taft and L. Cordes, "Optical Evidence for A Silicon-Silicon Oxide Interlayer", J. Electrochem. Soc. 126, 131 (1979).

13. D.E. Aspines and J.B. Theeten, "Spectroscopic Analysis of the Interface Between Si and Its Thermally Grown Oxide", J. Electrochem. Soc., 127, 1359 (1980).

14. M.E. Pedinoff, M. Braunstein, O.M. Stafsudd, "Strain Induced Anisotropy in As_2S_3, As_2Se_3, and ZnSe Films on KCl Substrates Via 10.6-μm and 0.6328-μm Ellipsometer Measurements and 0.6328-μm Reflector Measurements", Appl. Optics 18, 201 (1979).

15. R.M.A. Azzam and N.M. Bashara, Ellipsometry and Polarized Light, North Holland Publish. Co., N.Y., 1977.

16. McCrackin, F.L., E. Pasaglia, R.R. Stromberg, and H. Steinberg, "Measurement of the Thickness and Refractive Index of Very Thin-Films and the Optical Properties of Surfaces by Ellipsometry", J. Res. Natl. Bur. Stand. 67A, 363-277 (1963).

17. M.S. Abrhams, J. Blanc, C.J. Bulocchi, and W.E. Ham, "Shear Strain at Corners and Edges of Epitaxial Silicon on Sapphire," J. Appl. Phys. 46 652 (1978).

18. T.I. Kamins, E.S. Meieran, "X-ray Measurements of Stress in Thin Single Crystal Silicon Films", J. Appl. Phys. 44, 5064 (1973).

19. D. Den Engleston, "Ellipsometry of Anisotropic Films", J. Optical Soc. Am. 61, 1460 (1971).

20. K.B. Blodgett and I. Langmuir, "Built-up Films of Barium Stearate and Their Optical Properties," Phys. Rev., 51, 964 (1937).

21. A.E. Ennos, "Stresses Developed in Optical Film Coatings," Appl. Optics. 5, 51 (1966).

22. K. Kinosita, K. Nakamoto, K. Mari, K. Onovki, and K. Takenchi, "Mechanical Stresses in Vacuum Deposited Films of Ag, MgF_2, and ZnS," Jap. J. Appl. Phys. 4 (Suppl. 1), 340 (1965).

23. A.E. Hill and G.R. Hoffman, "Stress in Films of SiO," Brit. J. Appl. Phys. 18, 13 (1967).

24. R. Carpenter and D.S. Campbell, "Stress in Alkali Halide Films," J. Mater, Sci. 2, 173 (1967).

25. F.K. Rhinehart and R.A. Cogan, "Interface Stress of $Al_xGa_{1-x}As$-GaAs Layer Structures," J. Appl. Phys. 44, 3171 (1973).

26. Private communication, J. DeSmet.

27. R.W. Hoffman in Physics of Thin Films, Vol. 3, G. Hass and R.E. Thun, eds. Academic Press, N.Y. and London, 1966, pp. 211-273.

28. R.W. Hoffman, "The Mechanical Properties of Non-metallic Thin Films," U.S. Atomic Energy Commission, Contract No. AT 11-1-623 Technical Report No. 82, March 1975.

29. J.F. Nye, Physical Properties of Crystals, Oxford at the Clarendon Press, 1967, Chapter 13.

30. ibid, Chapter 8.

31. E. Klokholm, X-Ray Diffraction and Stress in Thin Films Symposium, IBM Thomas J. Watson Research Center, Yorktown Hts., New York (March 1969).

32. W. Primak and D. Post, "Photoelastic Constants of Vitreous Silica and Its Elastic Coefficient of Refractive Index", J. Appl. Phys. 30, 779 (1959).

33. R.M. Waxler, D. Horowitz and A. Feldman, "Precision Interferometer for Measuring Photoelastic Constants," Applied Optics 16, 20 (1977).

END

DATE
FILMED

6-81

DTIC